

Scientific report

*Regarding the implementation of the project PN-II-ID-PCE-2011-3-0762, no. 175/25.10.2011
Reduction of nanoparticle emissions by the optimization of residual combustion gases filtering processes
during the period October 2011 – December 2014*

The general interdisciplinary objectives of the project are:

- Mathematical modelling and numerical simulation of the behaviour of nanometric particle suspensions in fluid compressible environment – combustion gases – under the action of an electric field for describing nanoparticles capture,
- Experimental modelling and optimization of filtering processes, in order to reduce the nanoparticles emissions in the combustion gases,
- Development of a pre-feasibility study of the suggested product both from an economic perspective and in terms of an intervention through public policy, in order to estimate the intention of investing in nanometric particle filters.

Stage 2011 (October – December 2011)

Main objective:

- 1. *The build-up of a data basis containing the main theoretical and experimental results published in the field, consisting in documentation and classification of the bibliography based on specific criteria: theoretical, computational, experimental, nanoparticles analysis and characterization.***

We performed a database which contains a total of 60 journals containing 124 specialized articles starting with 1998, taken from international databases (American Institute of Physics, Institute of Physics, Science Direct, Springer Link, Taylor & Francis, Web of Science) made available by courtesy of UEFISCDI in the project ANELIS and University Library of the West University Timisoara.

Activities:

- Bibliographical study

1. The current situation concerning the field related to project

Nanometric particles have been a topic of special interest in the past two decades of scientific research. The harmful effect of nanosuspensions (< 100 nm) has become a more and more pressing issue on a global scale. Once inhaled, these toxic agents infiltrate into the blood very fast and cannot be eliminated, because the macrophages cells cannot identify them. Recent research [1-4] has shown that although raw materials may not be dangerous, they can become toxic under the form of nanoparticles.

At European level, in May 2008, has been adopted Directive on ambient air quality and cleaner air for Europe (Directive 2008/50 / EC). It is setting new air quality objectives for PM_{2.5} (fine particles) and aims at prevent the detrimental effects on the environment and health. Directive 2010/75 / EU of the European Parliament and of the Council of Europe on industrial emissions (emissions from stationary sources and emissions from electricity production) was adopted on 24 November 2010, entered in force at 6 January 2011 and must be transposed into national legislation by Member States until 7 January 2013. The program „Clean Air for Europe" and the program "Inspire" aims to reduce such pollution until 2020. Romania has implemented a large proportion of European legislation in environmental protection. The legislation passed (GD 541/2003; MAPPM Order 462/1993) dust emissions are limited to 30-50 mg / m³ for large combustion plants and 50 mg / m³ for other industry sectors, but regarding the process of nanoparticle filtration does not yet exist efficient solutions. Inhaled nanoparticles may generate free radicals, affect the DNA, and alter the genes, which leads to increased cancer risk and incidence of mutagenic and teratogenic-related phenomena. The main factors that cause nanoparticles pollution are industrial emissions (generated by waste incineration plants, metallurgy, cement factories, steam power stations etc.) and internal combustion engines.

All chemical compounds contained in the gases resulting from combustion processes are harmful effect on the atmosphere, biodiversity and human body. Spread of their both as nanoparticles adsorbed on carbon as well as the finely divided determine maintaining for long time as very fine suspension into the atmosphere and also the most direct assimilation pulmonary blood cell and these emissions. Generally, the

sources of polluting emissions are equipped with different filters; however, these filters capture only micron particles, while all nanoparticles escape in the air. Although the nanoparticles mass is smaller when compared with the micron particle mass, the size range of the former is at least for times higher than that of all other masses. Classical methods for handling (retention, separation) micrometer particles were tested in recent years and nanometric particles, most but without much success [3]. In the traditional particle-capture device, only a small part of the particles is collected and only when they attach to larger particles. Mechanical devices (cyclones, bag filters, sedimentation chambers) are not effective because of the low weight of the nanoparticles, and the chemical methods are slow and may change the nanoparticles composition during processing. Common Corona electrostatic filters have high micrometric particle retention efficiency (93-99%), but most nanoparticles escape in the air [2,4]. In the past years, the most promising nanoparticles manipulation methods are those based on dielectrophoresis (DEP) [4,5], the motion of matter caused by polarization effects in a non-uniform electric field. This does not require the particles to be charged (Figure 1). In non-uniform electric fields, dielectric particles move because of the interaction between the dipole moment induced in the particle and the electric field, having as result a translational force called dielectrophoretic force (\mathbf{F}_{DEP}). The dielectrophoretic force depends on the particles' size and conductivity, the dielectric constant of the particles and the medium, and the square of the current gradient [4-8].

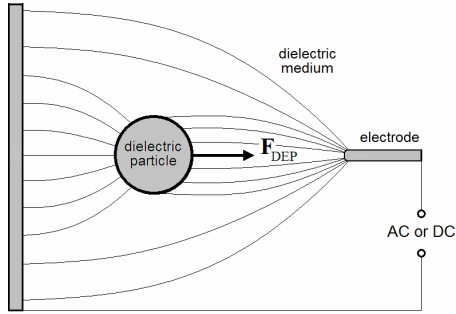


Figure 1: Electrically neutral particle in the presence of a spatially non-uniform electric field.

The dielectrophoretic force can be written as [4-7]: $\mathbf{F}_{DEP} = (\mathbf{m}(\omega) \cdot \nabla) \mathbf{E}$, where \mathbf{E} is the electric field, $\mathbf{m}(\omega) = 4\pi a^3 \epsilon_m k(\omega) \mathbf{E}$ is the induced dipole moment of the particle, ω is the angular field frequency, a the particle radius, and $k(\omega)$ the Clausius–Mossotti factor. In fluid media, the dielectrophoretic force, the nature of hydrodynamic forces (viscosity), weight, Archimedes, thermal, Brownian and quantum forces, determines the trajectory of a particle.

The total force on a polarizable particle in a nonuniform AC field can be written as the sum of a number of independently acting forces:

$$\mathbf{F} = \mathbf{F}_{DEP} + \mathbf{F}_{drag} + \mathbf{F}_{buoyancy} + \mathbf{F}_{thermal} + \mathbf{F}_{brownian} \quad [7].$$

Where: \mathbf{F}_{DEP} is the dielectrophoretic force, \mathbf{F}_{drag} is the hydrodynamic drag force, $\mathbf{F}_{thermal}$ the thermal force and $\mathbf{F}_{brownian}$ is the force due to the brownian motion of the particles.

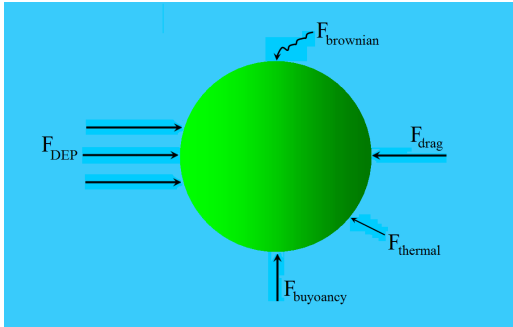


Figure 2: Forces exerted on a particle moving in fluid, under the influence of dielectrophoresis

1.1 Mathematical modeling of dielectrophoresis

To determine the electric field and dielectrophoretic forces start from calculation of electric potential for geometry and boundary conditions corresponding to the network of electrodes.

Using the notation of the phase, frequency oscillating potential ω is written as $V(\mathbf{x}, t) = \text{Re}\{\tilde{V}(\mathbf{x})e^{j\omega t}\}$, where $j = (-1)^{1/2}$, vector \mathbf{x} describes the spatial coordinates, $\text{Re}\{\}$ indicates the real part and the symbol “ \sim ” is phasor $\tilde{V} = V_R + jV_I$, with V_R si V_I respectively the real and imaginary part of the electric potential. The two components of potential satisfies Laplace's equation: $\nabla^2 V_R = 0$ and $\nabla^2 V_I = 0$. Bulk density time-averaged force acting on the particle dipole is $\langle \mathbf{F} \rangle = 3/2 \epsilon_m \text{Re}\{\tilde{k}(\omega) \tilde{\mathbf{E}} \cdot \nabla \tilde{\mathbf{E}}^*\}$ [8,9], where $\tilde{\mathbf{E}} = -\nabla \tilde{V} = -\nabla(V_R + jV_I)$ is the electric field phasor, “ $*$ ” indicates the complex conjugate, Clausius-Mossotti factor is $\tilde{k}(\omega) = (\tilde{\epsilon}_p - \tilde{\epsilon}_m) / (\tilde{\epsilon}_p + 2\tilde{\epsilon}_m)$, $\tilde{\epsilon}_p$ si $\tilde{\epsilon}_m$ and the absolute permittivity of the particle and the

environment respectively, sizes dependent dielectric properties of the particle and particle geometry and environment.

To prevent the calculations with numerical values that stretch on a very large range in practice using a dimensionless form of equations. In our case, using a scaled value of the electric potential applied to the signal amplitude V_0 and reporting reference distances at a distance d (for example the distance between the electrodes) we obtain the expression dimensionless of power density:

$$\langle \mathbf{F} \rangle = \langle \mathbf{F}_{DEP} \rangle + \langle \mathbf{F}_{twDEP} \rangle = 3/4 \epsilon_m \tilde{k}_r (V_0^2 / d^3) \nabla' (|\nabla' V_R'|^2 + |\nabla' V_I'|^2) - 3/2 \epsilon_m \tilde{k}_i (V_0^2 / d^3) (\nabla' \times (\nabla' V_R' \times \nabla' V_I'))$$

where $V'_R = V_R/V_0$, $V'_I = V_I/V_0$ si $\mathbf{x}' = \mathbf{x}/d$, and lower indices r and i highlights the real and imaginary that Clausius-Mossotti factor [8-10]. The first term is called DEP force and depends on the the non uniformity of the field created by the electrodes. It suggest that dielectrophoretic force can be used to separate particles due to their different polarization depending on the environment and the particle permittivity (the sign of $\tilde{k}_r(\omega)$ depends on the permittivity, conductivity and frequency of the signal applied to the electrodes). The second term is called force twDEP (traveling wave dielectrophoresis) and is not null if the electric field shows the spatial variation of phase. Such situations are found only in the case of alternating electric fields. In certain geometries, twDEP force can be used for particle separation by different properties / sizes [4-8]. The correct determination of dielectrophoretic force is done by numerical solution of the Laplace equation for the electric potential on a realistic geometry and boundary conditions appropriate. Due to the periodicity of the electrode system (Figure 3) - where w denotes the width of the electrodes, d the distance between two electrodes, h the separation chamber height (range considered) - dielectrophoretic force calculation can be performed on a single "unit cell". An example of geometry considered in the numerical solution of the problem, and specific boundary conditions are presented in Figure 4 [8-10].

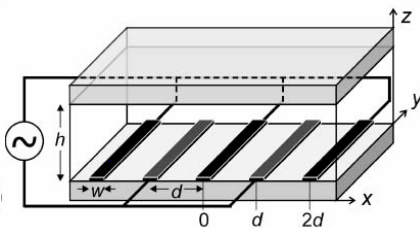


Figure 3: DEP separation chamber. System supported by a glass electrode.

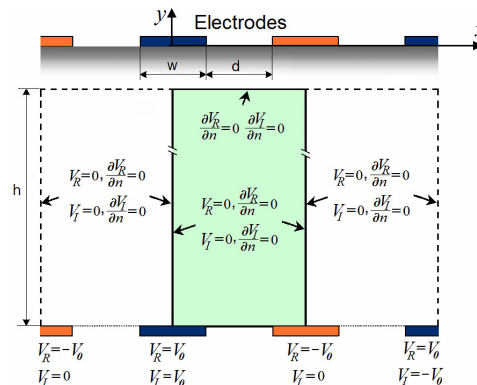
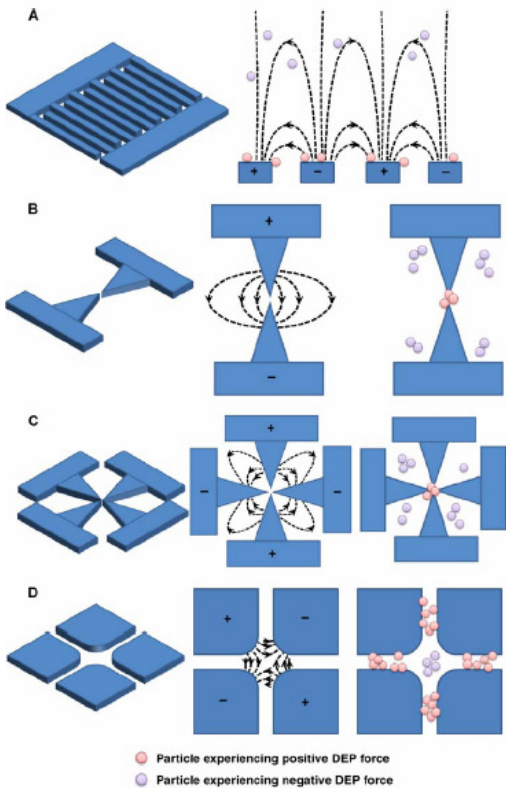


Figure 4: Domain and boundary conditions for calculating electric potentials

Can also be used for other types of boundary conditions, more convenient in terms of numbers but less realistic and analytical approach to problem variants [4,8]. Dielectrophoretic forces depend on the spatial coordinates, and are a strong variation near the electrode edges where field gradients are maximal.

1.2 The current situation on the experiment and applications in the field

Dielectrophoresis present a number of applications for the manipulation and analysis of micro- and nano-particles. The fundamental method by manipulation consists in capturing of particles in areas of maximum intensity of the local electric field. Such methods have been used successfully to capture micro particles and living cells [5,6]. More importance terms of application of methods of dielectrophoretic separation. In this system, the components of a dual suspension are separated in the minimum, respectively the maximum zones of the electric field. Separation method was successfully used to separate micro-particles, mineral particles, bacteria, animal cells, red cells or cancer cells live cells cell death. The first disadvantage in this conFigureation consists in the necessity of having a relative difference of 50% between particle excitation frequencies. This problem was solved in part by using the technique of "traveling-wave DEP" (twDEP), used to capture and separation of viruses or cancer cells. Methods of type "field flow fractionation" (DEP-FFF) were used to position the particles in a fluid flow using dielectrophoresis methods. DEP FFF is important because it allows the manipulation submicron-sized particles, which Brownian motion has an impact on the position. DEP-FFF is used in systems that contain latex microspheres, stematic cells or red blood cells [11]. Another method may also be used to focus a stream of particles or cells in a fluid in movement in dielectrophoresis deflection. An important factor in determining the possible applications of



dielectrophoresis is the geometry of the devices used [6,7]. In practice, using a number of standard models illustrated in Figure 5. The choice of device and its dimensions are determined primarily by the distribution of electric field or particle properties to be analyzed. In terms of practical applications, the main use of DEP is that of micro-biology [12]. Dielectrophoresis was used for handling chains of DNA, proteins and viruses. A DNA chain by $16.5 \mu\text{m}$ was immobilized using a set of electrodes by $15 \mu\text{m}$. In a similar experiment, DEP has been used for capture of a DNA chain using a four electrode configuration sizes between 5 and $50 \mu\text{m}$. Capturing and analyzing DNA were performed in $2 \mu\text{m}$ size devices, where DEP was used to remove the impact of Brownian forces. One of the first examples of dielectrophoretic manipulation of proteins refers to the avidin molecules. The device used in this case consisting of a parallel electrode configuration and size separation $2 \mu\text{m}$. Similar results have been reported when handling and separation of viruses, size configurations typically used in the field that it is up to $4 \mu\text{m}$. In the field, nanoscopic, reported a number of successes in capturing bacterial cells (typical size around 800 nm) using a circular DEP configuration with dimensions between 230 and $780 \mu\text{m}$ (Figure 6) [6]. Due to the compact dimensions DEP devices,

they have become a major candidate for technology development "lab-on-a-chip" devices micro- and nanoscopic that integrates instrumentation needed to perform a series of tests [13]. A practical example of such a device is illustrated in Figure 7. This type of configuration is used in the separation and transportation of cells or combination of drugs. Typical dimensions are millimeters devices but can reach sizes of the order of centimeters. A number of models have been proposed to handle the conductive particles and dielectric particles in suspension and manipulating the separation of particles from a flowing fluid. With the evolution of the degree of miniaturization, integrated DEP devices were used to control typical particle size of 93 nm (Figure 8).

Another set of applications of electrophoresis occurs in nanotechnology, particularly in the assembly of new devices nanoscopic dimensions. In this context, the DEP has been used successfully for the handling and control of the nano-wire or carbon nano-tubes [11-13].

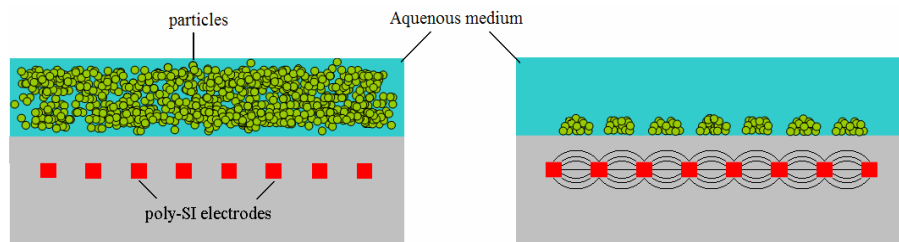


Figure 7: Scheme of a device lab-on-a-chip.

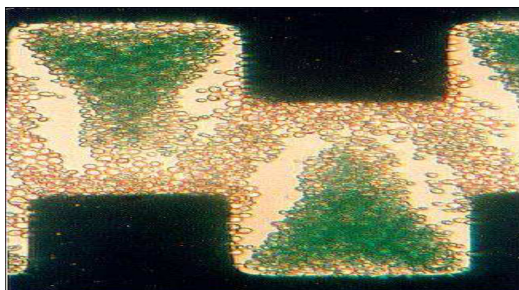


Figure 8: Collection of nanoparticles with DEP.

2. Subsequent steps, prospects

Because at present there is no single model that describes the behavior of nanoscale suspensions in fluid media under the dielectrophoresis action, the project aims to achieve in the next stage a mathematical model that considers all the forces governing the electrohydrodynamics of nanoparticle. The dielectrophoretic, viscosity, Brownian forces, thermal and quantum nature depend on their physical properties of nanoparticle, the environmental fluid and electric applied field. The model will then be implemented numerically in order to obtain know-how of making devices for handling nanoparticles (retention, separation) for class sizes and / or different physical properties.

Conclusions

The bibliographic study and technical solutions analysis conducted for current implementation represent a set based available on the scientific technical requirements and met by the project team in the next stages, where they checked the hypothesis formulated, in purpose of fulfilling the project objectives.

References:

- [1] Office for Official Publications of the European Communities: *Ambient air pollution by As, Cd and Ni compounds*, Position Paper, Luxembourg (2001), ISBN 92-894-2054-5.
- [2] D. Rickerby, M. Morrison: *Report from the Workshop on Nanotechnologies for Environmental Remediation*, JRC Ispra 16-17, April (2007).
- [3] A.D. Maynard, E.D. Kuempel: *Airborne nanostructured particles and occupational health*, J. of Nanoparticle Research **7** (2005).
- [4] M. Lungu, A. Neculae, M. Bunoiu: *Some considerations on the dielectrophoretic manipulation of nanoparticles in fluid media*, J. of Optoelectronics and Advanced Materials **12** (2011).
- [5] R. Pethig: *Review Article-Dielectrophoresis: Status of the theory, technology, and applications*, Biomicrofluidics **4**, (2010).
- [6] C. Zhang, K. Khoshmanesh, A. Mitchell, K. Kalantar-Zadeh: *Dielectrophoresis for manipulation of micro/nano particles in microfluidic systems*, Anal Bioanal Chem **396**, (2010).
- [7] A. Castellanos, A. Ramos, N. Gonzales, N. Green, H. Morgan: *Electrohydrodynamics and dielectrophoresis in microsystems: scaling laws*, J. Phys. D: Appl. Phys., Vol. **36**, (2003).
- [8] S. Shklyaeu, A.V. Straube, *Particle entrapment in a fluid suspension as a feedback effect*, New Journal of Physics **10**, (2008).
- [9] N.G. Green, A. Ramos, H. Morgan: *Numerical solution of the dielectrophoretic and travelling wave forces for interdigitated electrode arrays using the finite element method*, J. of Electrostatics **56**, (2002).
- [10] Yuan Lin: *Numerical modeling of dielectrophoresis*, Technical Reports from Royal Institute of Technology KTH Mechanics SE-100 44 Stockholm, Sweden, (2006).
- [11] S.J. Dickerson: *Design of 3D Integrated Circuits for Manipulating and Sensing Biological Nanoparticles*, PhD Thesis, University of Pittsburgh, (2007).
- [12] B. H. Lapizco-Encinas, M. Rito-Palomares: *Dielectrophoresis for the manipulation of nanobioparticles*, Electrophoresis **28** (2007).
- [13] www.nanoforum.org

Main objectives:

2. *The build-up of a mathematical model for describing the studied system (suspensions of nanometric particles in a fluid medium, subject to an electric field)*

Activities:

- **The founding the system of equations which governs the system dynamics, the computational domain, the specific initial and boundary conditions**

The mathematical model was built to describe the behavior of a suspension of nanoparticles in a fluid media subjected to a nonuniform field (dielectrophoresis), under the action of gravity, viscosity.

According to general considerations presented in the report of stage 2011, the average force acting on a dielectric particle in nonuniform electric field dielectric comprises two independent contributions (the subscripts r and i denote the real and imaginary parts):

$$\langle \mathbf{F} \rangle = \frac{3}{4} \epsilon_m K_R \nabla |\tilde{\mathbf{E}}|^2 - \frac{3}{2} \epsilon_m k_I \nabla \times (\mathbf{E}_R \times \mathbf{E}_I) \quad (1)$$

The first term relates to an electric field which is non-uniform in magnitude but does not exhibit any phase variation. The second term of equation (1) is non-vanishing if the electric field has a spatially dependent phase, and the dielectrophoresis resulting from such an electric field phase gradient is known as *traveling wave dielectrophoresis (twDEP)*. The *Clausius–Mossotti (CM)* factor is given by:

$$\tilde{K}(\omega) = \frac{\tilde{\epsilon}_p - \tilde{\epsilon}_m}{\tilde{\epsilon}_p + 2\tilde{\epsilon}_m} \quad (2)$$

with $\tilde{\epsilon}_p$ and $\tilde{\epsilon}_m$ the absolute complex permittivity of the particle and the medium, respectively, and it depends on the dielectric properties of the particles and the medium, as well as the geometry of the particles. The complex permittivity is $\tilde{\epsilon} = \epsilon' - i\epsilon''$ where ϵ' and ϵ'' are the real and imaginary components of the complex dielectric permittivity, which may be written in the Debye form:

$$\epsilon' = \epsilon_\infty + \frac{\epsilon(0) - \epsilon_\infty}{1 + \omega^2 \tau^2}, \quad \epsilon'' = \frac{\sigma}{\omega \epsilon_0} + \frac{[\epsilon(0) - \epsilon_\infty] \omega \tau}{1 + \omega^2 \tau^2} \quad (3) (4)$$

where σ is the electric conductivity of the particle or medium and τ is the relaxation time. From the Debye theory [6] it is known that the relaxation time is correlated to the frequency f_{max} , at which ϵ'' has a maximum, by the relation, $2\pi f_{max} \tau = 1$. Also, in Eqs. (3) and (4), $\epsilon(0)$ is the permittivity at frequencies much smaller than f_{max} and ϵ_∞ is the permittivity at frequencies much larger than f_{max} [7]. For systems with more than one relaxation time, both equation (3) and equation (4) are sums of terms corresponding to different relaxation processes [7]. By introducing in Eq. (2) the complex form of dielectric permittivity of particle, $\tilde{\epsilon}_p = \epsilon'_p - i\epsilon''_p$, respectively, dielectric permittivity of medium, $\tilde{\epsilon}_m = \epsilon'_m - i\epsilon''_m$, we can determine the real, $\text{Re}[\tilde{K}(\omega)]$ and imaginary, $\text{Im}[\tilde{K}(\omega)]$ components, of the CM factor. Result following relationships:

$$\text{Re}[\tilde{K}(\omega)] = \frac{\epsilon'^2_p + \epsilon''^2_p + \epsilon'_p \epsilon'_m - 2\epsilon''^2_m + \epsilon''_m (\epsilon''_p - 2\epsilon''_m)}{\epsilon'^2_p + \epsilon''^2_p + 4\epsilon'_p \epsilon'_m + 4\epsilon''^2_m + 4\epsilon''_m (\epsilon''_p + \epsilon''_m)} \quad (5)$$

$$\text{Im}[\tilde{K}(\omega)] = \frac{3\epsilon''_p \epsilon'_m - 3\epsilon'_p \epsilon''_m}{\epsilon'^2_p + \epsilon''^2_p + 4\epsilon'_p \epsilon'_m + 4\epsilon''^2_m + 4\epsilon''_m (\epsilon''_p + \epsilon''_m)} \quad (6)$$

From equations (5) and (6) we can observed that the real and imaginary components of the Clausius–Mossotti factor, depends on the dielectric properties of the particle and medium, and of the frequency of the applied field. The frequency dependence of this factor determines dependence in frequency of DEP force, which is unique to a particular particle type. Therefore, we can use dielectrophoresis as an effective means for particle separation, solely according to their dielectric properties and size. Being a measure of the relative permittivity between the particle and the surrounding medium, the CM factor determines the sign of the DEP force: when $\text{Re}[\tilde{K}(\omega)] > 0$, the particle is more polarizable than its surrounding medium and is attracted toward the locations of maximum electric field intensity and repelled from the zones of minimum, phenomenon known as positive dielectrophoresis (pDEP). The opposite occurs when $\text{Re}[\tilde{K}(\omega)] < 0$, referred to as negative dielectrophoresis (nDEP).

For a homogeneous medium, the two components of the electrical potential $\tilde{V} = V_R + jV_I$ satisfy the Laplace equation:

$$\nabla^2 V_R = 0, \nabla^2 V_I = 0. \quad (7)$$

The two components of force (1) can be expressed as [1,4]:

$$\langle \mathbf{F}_{DEP} \rangle = \frac{3}{4} \epsilon_m K_R \nabla (|\nabla V_R|^2 + |\nabla V_I|^2), \text{ respectiv } \langle \mathbf{F}_{twDEP} \rangle = -\frac{3}{2} \epsilon_m K_I (\nabla \times (\nabla V_R \times \nabla V_I)) \quad (8)$$

The real part of the Clausius-Mossotti factor $K_R(\omega)$ gives the DEP force in the direction perpendicular to the electrode array, while the imaginary part $K_I(\omega)$ gives the twDEP force in the parallel direction.

Figure 9 presents two typical structures of microfluidic devices with interdigitated bar electrodes at the bottom surface used in dielectrophoretic separation. The first corresponds to DEP separation, while the second to twDEP separation:

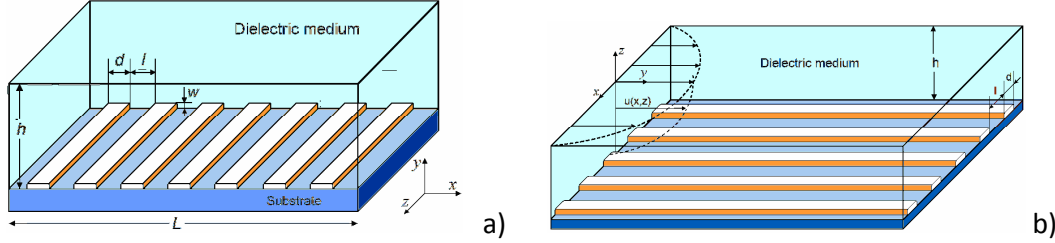
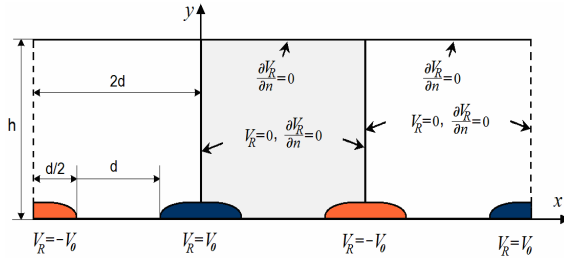


Figure 9: Schematic of the microfluidic devices with interdigitated bar electrodes at the bottom surface used in dielectrophoretic separation: a) DEP separation, b) twDEP separation.

Figure 10 is a schematic representation of the computational domain with boundary conditions for the real part (V_R) of the electric potential. The solid lines indicate the basic unit cell. Neumann boundary conditions are used on the surface of the electrodes and mixed, Dirichlet and Neumann, on the sides of the unit cell. The boundary conditions for the imaginary potential are similar. In the literature is neglected physical



thickness of the electrodes (as in the report stage 2011), but in our mathematical model we used a more realistic description of the problem, which takes into account the shape and thickness of the electrodes [3,4,12].

Figure 10: Schematic representation of the computational domain with boundary conditions for the real part (V_R) of the electric potential. The solid lines indicate the basic unit cell.

The macroscopic behavior of a suspension of spherical particles in a dense and viscous fluid could be modeled considering the mechanical equilibrium between an external force \mathbf{F} and the Stokes drag [1,4]:

$$\mathbf{v} = \mathbf{u} + \frac{2a^2}{9\eta} \mathbf{F}, \text{ unde: } \nabla \mathbf{u} = 0; \frac{\partial \varphi}{\partial t} + \nabla \cdot \mathbf{j} = 0, \text{ unde: } \frac{\partial \varphi}{\partial t} + \nabla \cdot \mathbf{j} = 0. \quad (9)$$

Here \mathbf{u} and \mathbf{v} are the fluid and particle velocities, respectively, a the particle radius, η the viscosity of the fluid, t the time, \mathbf{j} the particle flux, D the diffusion coefficient of the particles.

A representation of the domain for determining the concentration field is given in Figure 11. If neglect the electrode thickness, fluid flow profile can be considered as Poiseuille type [4,5,12], but in case it takes into account the geometry of the electrodes, the velocity field is calculated numerically by solving the Navier-Stokes equation by imposing the condition of real fluid adhesion to walls and electrodes [3-5].

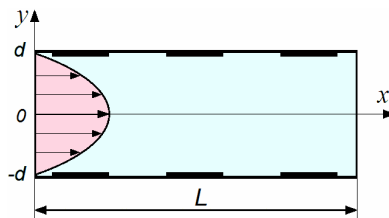


Figure 11: Schematic representation of macroscopic domain to calculate the concentration field. The fluid flow is Poiseuille type.

Using the scales of $d, d^2/D, D/d$ and φ_0 (the initial average volume fraction) for the length, time, velocity and particle volume fraction,

respectively, the problem is expressed in terms of dimensionless variables by the following system of equations [9]:

$$\mathbf{v}' = \mathbf{u}' + Q\mathbf{F}', \text{ unde: } \nabla \mathbf{u}' = 0; \quad \frac{\partial \phi'}{\partial t'} + \nabla \cdot \mathbf{j}' = 0, \text{ unde: } \mathbf{j}' = \phi' \mathbf{v}' - D \nabla \phi'. \quad (10)$$

The prime symbol above denotes the dimensionless quantities, $Q = 2a^2 F_0 d / 9\eta D$ with F_0 a measure of the intensity of the external field

- The establishment of the parameter values appearing in the system

For the parameters of the problem were considered typical values that allow comparison of our results with those from the literature and finally validating numerical codes. During the comparison/validation stage we considered particles with characteristic size $a=200\text{nm}$ in water ($\eta=10^{-3}\text{kgm}^{-1}\text{s}^{-1}$, $\rho=10^3\text{kgm}^{-3}$, $D \approx 10^{-12}\text{m}^2\text{s}^{-1}$, $\epsilon_m \approx 80$). The characteristic length of the device is $d = 50\mu\text{m}$. For a imaginary part of the Clausius-Mossotti factor $k_I \approx 0.6$ (corresponding to latex particles in water), an amplitude of the electric potential $V_0 \approx 1\text{V}$ and a traveling wave with $\lambda = 400\mu\text{m}$, we obtain for the dimensionless parameter in equation (11a) a typical value of $Q \approx 0.2$. The fluid flow in the microchannel is assumed to be laminar and described by a Poiseuille profile with a typical value of $1\mu\text{m/s}$ for the maximum flow velocity.

3. The numerical implementation of the mathematical model

Activities:

- The build-up of the program for the simulation of nanoparticles dynamics in electric field. The validation of the program by comparisons with previously published results

The programs used for the numerical implementation of the mathematical model were written using FreeFEM ++, a solver for equations based on finite element method. To validate programs have used particular cases of our problem, admitting analytic solution or resolved in previously published papers in the field. Validation program for calculating dielectrophoretic force was achieved in the particular case of neglect electrode geometry [6,8,9]. Was chosen geometry described by dimensions $d_1=d_2=d=50\mu\text{m}$ and $h=10d$ and boundary conditions as in Figure 10.

The results obtained for the amplitudes of vectors $\nabla'(|\nabla'V_R'|^2 + |\nabla'V_I'|^2)$ and $\nabla' \times (\nabla'V_R' \times \nabla'V_I')$, proportional with the adimensional values of the forces DEP and twDEP given by equations (4) are in a very good concordance with the results from the literature. A more accurate quantitative validation of the calculation force program was made by comparing numerical solutions calculated with our program with an analytical solution proposed in the literature and show a perfect concordance in [8].

- Numerical study on the mobility and dispersion rate of the nanoparticles in fluid medium subject to electric field in order to control their retention or separation

To study the effect of particle size on the transport process, the simulations have been conducted with particles radii between 100 and 300 nm. The results for the concentration field in the case of particles with radii $a = 100\text{ nm}$ and $= 200\text{ nm}$ are shown in Figure 6 [8,9]. The results show that as the particle size decreases, the intensity of dielectrophoretic force acting on them decreases, both pDEP and NDEP forces.

Study of the influence of the physical properties of the particles and the fluid was made by the parameter Q , which contains both characteristics of fluid expression ($\eta, \rho, D, \epsilon_m$), and particles (radius a , Figure 12 a). The influence of Q parameter on the field of concentration is shown in Figure 12b). In the case of pDEP and the NDEP, the results show that as the parameter Q increases (a phenomenon that can be produced by increasing the supply voltage or decrease in viscosity, diffusion coefficient, distance characteristics, or particle radius) the value of dielectrophoretic force increases too.

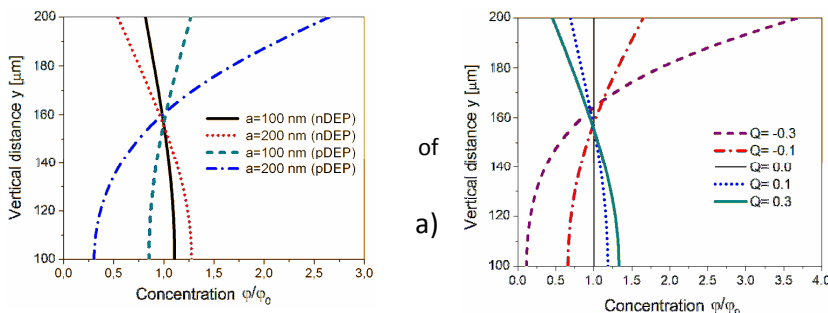


Figure 12: Calculated concentration profiles ϕ / ϕ_0 as a function of the vertical distance from the bottom electrodes, for several values of particle size a) and Q parameter b)

b)

A detailed study of the effect of electrode geometry on dielectrophoretic force is shown in [7,8]. Another important phase of our study is the calculation of particle trajectories subjected to DEP force [8,9]. To determine the trajectories, was integrated equation of motion $\mathbf{x} = \mathbf{x}_0 + \mathbf{v}_0 t + 1/2 \mathbf{a} t^2$ for different initial positions of the particles. The results of simulations performed for the geometry in Figure 10 confirm the estimated behavior of particles under the influence of dielectrophoretic forces: if pDEP particlele are attracted to the edges of the electrodes (Figure 13), where the particles are rejected by nDEP microcanalului center (Figure 13b), so DEP force acts in the vertical direction. Similar calculations show that the force twDEP produce oscillatory movements or straight, having as effect the transverse displacement of the particle.

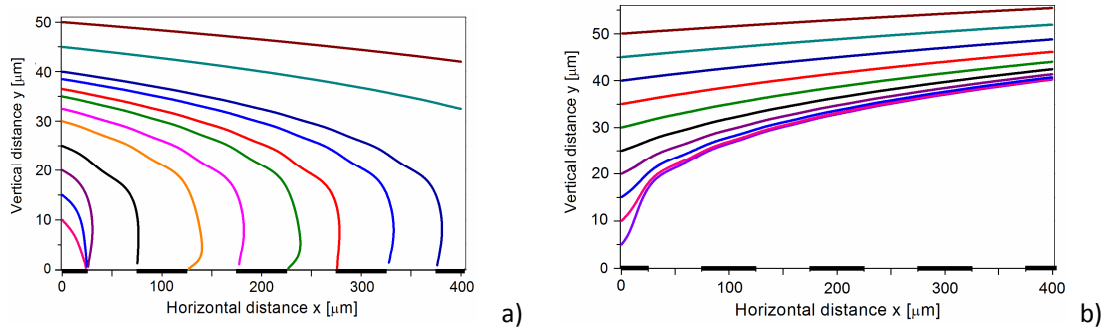


Figure 13: Calculated trajectories of particles with radius $a=200\text{nm}$ in case of positive DEP a) and negative DEP b). Ordinate shows vertical launch point of particles.

Figure 14 presents the vertical variation taken for $x=0$ (the electrode centre to the left of the domain), $x=0.25d$ (in the electrode body) $x=0.5d$ (the electrode's edge) and $x=d$ (the middle of the domain). As we can see, increasing the height of the electrodes leads to a translation of the DEP force, which causes it to slightly increase but does not affect the shape of its variation.

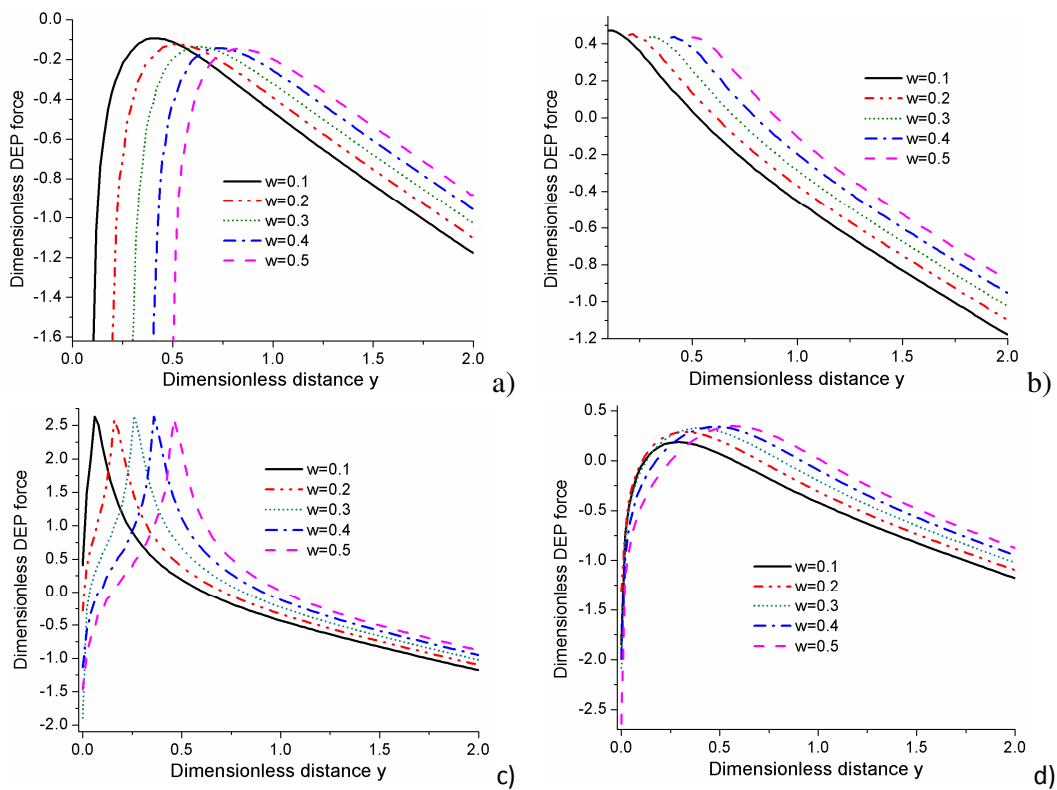


Figure 14: Vertical variation of the DEP force for electrodes with rectangular shape ($d_1 = d_2 = d$) and different heights w at: a) $x = 0$, b) $x = 0.25d$, c) $x = 0.5d$ and d) $x = d$.

The effect of dielectrophoretic forces on the suspension macroscopic scale was studied by integrating mass transport equation (11). For the expression of dielectrophoretic force can be considered an analytical

expression [8], or for a more realistic case, the value calculated numerically [14,15]. The applied voltage can change the value of parameter Q by increasing or decreasing the amplitude, Q increases or decreases by a quadratic law. In addition, by changing the frequency of the applied signal, the sign of Q can be changed. In Figure 14 are shown two examples calculated stationary concentration camps. Concentration profiles results show particle accumulation near the border for $Q > 0$ or in center of the microchannel for $Q < 0$, corresponding to pDEP and nDEP respectively.

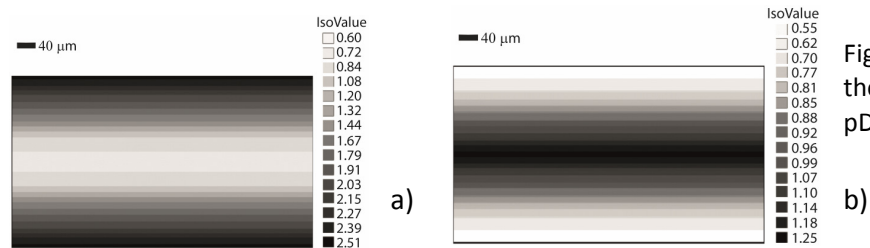


Figure 14: Numerical results regarding the stationary concentration field for a) pDEP ($Q = +0.2$), b) nDEP ($Q = -0.2$).

The effect of flow rate on the concentration has been studied in [18]. The calculations were made taking into consideration electrode geometry. Stationary concentration fields calculated at two different speeds of the fluid flow ($v = 1$ and $v = 100$) for $Q=0.2$ (pDEP) are presented in the results of stage 2013 and highlights the role that has the fluid flow velocity on the particle carrier .

4. Dissemination of the obtained results.

At the end of this stage was created a website of the project at the address: www.nanodep.com, containing the name and purpose of the project, the results obtained so far, team members, contacts and various useful information on handling nanoparticles in fluid media under the action of dielectrophoresis. The results obtained in stage 2012 were disseminated in international conferences and published or submitted for publication in international journals as listed at the end of the report of Stage 2013, used also as references in the text of the report.

Conclusions

The results obtained by numerical simulations based on the proposed mathematical model shows that dielectrophoretic forces can be successfully used in handling micro and nanoparticles. Based on these results we can better understand the physical processes that occur inside the experimental device and also can obtain an optimal set of parameters for its operation. A discussion on the effectiveness of a device dielectrophoretic separation is shown in the next stage.

Main objectives:

5. Numerical simulation of the behavior of suspensions of nanoparticles in the flue gas under the action of electric field, in order to retain them

Activities:

- The study of the influence of the physical properties of the particles and fluid.

Determining the trajectories of particles with different sizes and concentration fields under the action of electric field applied using electrodes of different forms, depending on the nature of the particles and fluid medium, at different frequencies.

- Finding the parameters of the system for an optimal trapping of the nanoparticles.

Identification the set of physical and chemical parameters of the system (shape and location of electrodes, particle size, frequency of the applied voltage, material characteristics of substances used) that lead to optimization of particle trapping.

The behaviour of nanoparticles having different dimensions inside a microfluidic separation device under dielectrophoresis was investigated by analyzing the following parameters: the fluid flow velocity, the voltage applied on the electrodes, the geometry of the electrodes, the geometry of the separation device, particle trajectories, the frequency dependence of the CM factor of the particles. The set of geometric parameters of the device, the electric parameters (applied voltage, frequency of the applied signal) and physico-chemical parameters (material characteristics of the substances used) of the problem, correlated to the nature and dimension of particles can lead to the optimization of the nanoparticle capture process.

Performed activities:

- The study of the influence of the flow velocity on the nanoparticle distribution inside the microfluidic device

The analysis was performed by determining the concentration distribution for different flow intensities, corresponding to dimensionless values for velocity ranging in the domain 1-1000. These values correspond to a device having the dimensions $h = 200 \mu\text{m}$ and $L = 1000 \mu\text{m}$ (see Figure 9a), and to flow velocities inside it ranging from 1 to 1000 $\mu\text{m/s}$. In Figures 15 and 16 are presented the calculated concentration distributions for two values of the fluid flow velocity ($v=1$ and $v=100$), for $Q = 0.2$ (p -DEP) and $Q = -0.2$ (n -DEP), respectively. The results show that the suspended nanoparticles tend to concentrate on the walls in the case of positive dielectrophoresis (p DEP) or in the center of the flow channel, in the case of negative dielectrophoresis (n DEP). The effect of the flow velocity is clearly visible.

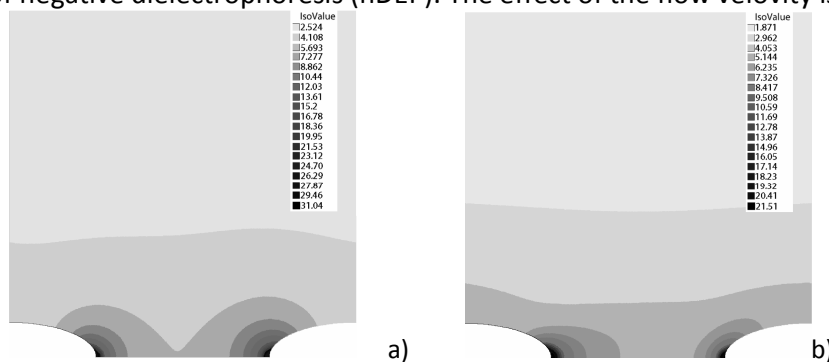


Figure 15: Calculated concentration field for pDEP ($Q=0.2$) at $v=1$ a), and $v=100$ b).

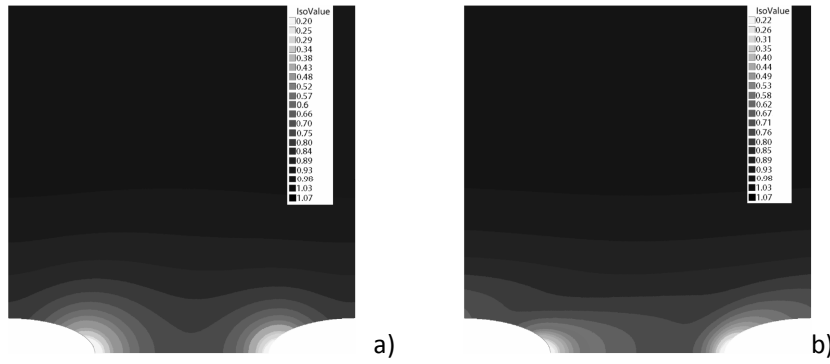


Figure 16: Calculated concentration field for nDEP ($Q = -0.2$) at $v = 1$ a), and $v = 100$ b).

A more refined analysis of the stationary concentration field was performed for different positions inside the separation device. The dimensionless coordinates $x = 0$, $x = 0.5$ and $x = 1$, respectively, correspond to the left margin of the computation domain, the right margin of the electrode and the middle of the gap between the electrodes, respectively. The Figures 17a and 17b present the vertical variation of the calculated concentration for different horizontal coordinates, in the case of pDEP, while Figures 18a and 18b refer to the case of nDEP, for dimensionless flow velocities $v = 1$ and $v = 100$.

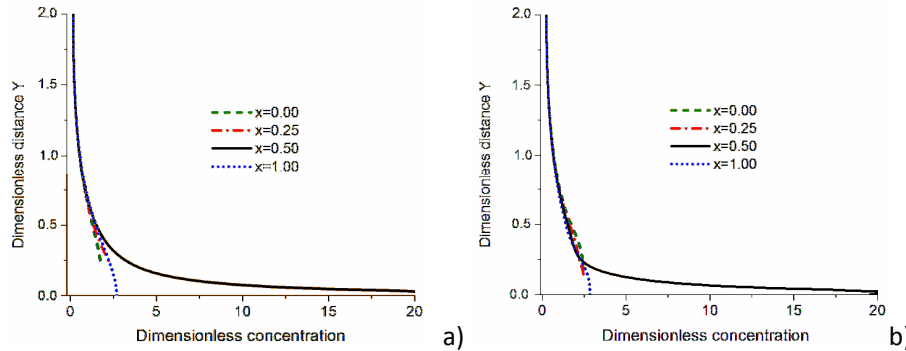


Figure 17: Concentration variation with height (pDEP, $Q = 0.2$) for $v = 1$ a) and $v = 100$ b).

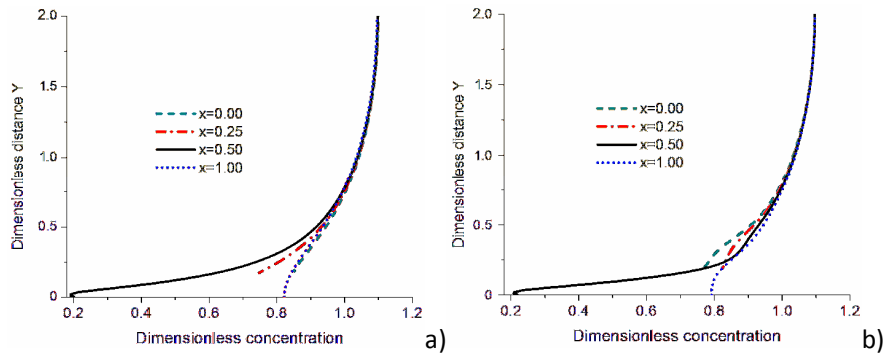


Figure 18: Concentration variation with height (nDEP, $Q = -0.2$) for $v = 1$ a) and $v = 100$ b).

- **The computation of the concentration fields for the suspended nanoparticles in the microfluidic filtration device; the analysis by specific parameters of the separation process.**

At this step, the numerical study deals with the computation of the concentration field for the nanoparticles suspended in flue gas, inside a microfluidic separation device. Because the carrying fluid is a gas, for which $\epsilon_r \sim 1$, only the pDEP component of the dielectrophoretic force is considered. The results were analysed by using three new parameters, called *Recovery*, *Purity* and *Separation Efficiency*, correlated with the concentration field. These parameters offer a more suggestive characterization of the separation capabilities of the microfluidic device. The numerical simulations were performed with the FreeFEM++ and COMSOL softwares, both based on the finite element method. For the computation of the dielectrophoretic force we solved the Laplace equations (7) for the real and imaginary parts of the electric

potential phasor, together with the associated boundary conditions (presented in Figure 19), for the particular case $d=l=30\ \mu\text{m}$ and $H=2d=60\ \mu\text{m}$.

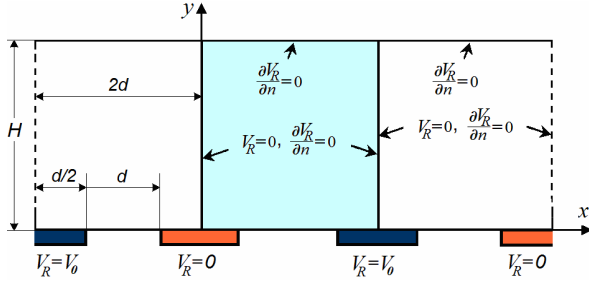


Figure 19: The geometry of the computational domain and the associated boundary conditions for the real part of the electric potential phasor, V_R .

The variation of the amplitude of the vector $\nabla'(|\nabla'V_R|^2 + |\nabla'V_I|^2)$, proportional to the dimensionless DEP force, is presented in Figure 20:

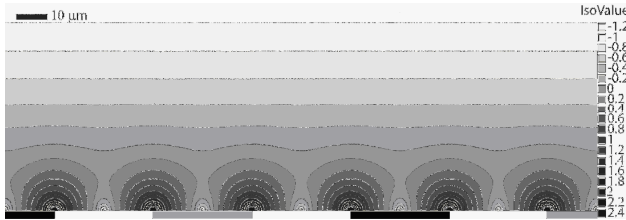


Figure 20: The calculated dimensionless DEP force in logarithmic scale, highlights a periodic variation.

Based on the periodic behaviour of the DEP force, we will consider next the analytical model given by equations (10). For simulating the behaviour of the suspended nanoparticles in flue gas inside the separation device, the equations (9) and the force (10) are solved for different values of the parameter Q , which describes the global influence of the physical quantities involved in the separation process: the applied voltage on the electrodes, particle radius, their permittivity. For obtaining a reference value of this parameter, we considered a suspension of particles of radius $a=100\ \text{nm}$ in air, the real part of the Clausius-Mossotti factor, $K_R=1$, for the suspended particles, the amplitude of the applied voltage on the electrodes $V_0=10\ \text{V}$ and the value of the travelling wave $\lambda=120\ \mu\text{m}$. The obtained value of the dimensionless wave number is $b=\pi$ and $Q\approx 1$. In Figure 21 one present the correlation between the applied voltage V and the nanoparticle radius, for different values of the parameter Q .

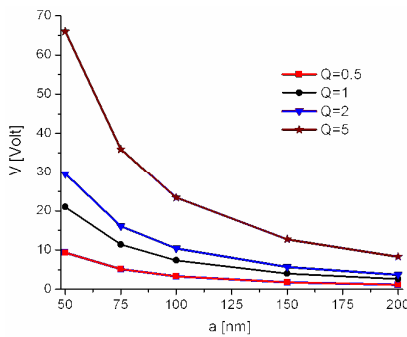


Figure 21: The correlation between the applied voltage amplitude V and the nanoparticle radius a , for different values of the parameter Q .

In Figure 22 are shown the calculated concentration field for suspended particles under positive dielectrophoresis (particles are attracted to the electrodes) for $Q=1$ ($a=100\ \text{nm}$, $K_R=1$, $V_0=10\ \text{V}$, $\lambda=120\ \mu\text{m}$), the red rectangle delimiting the zone of interest which will be considered next for the estimation of separation process:

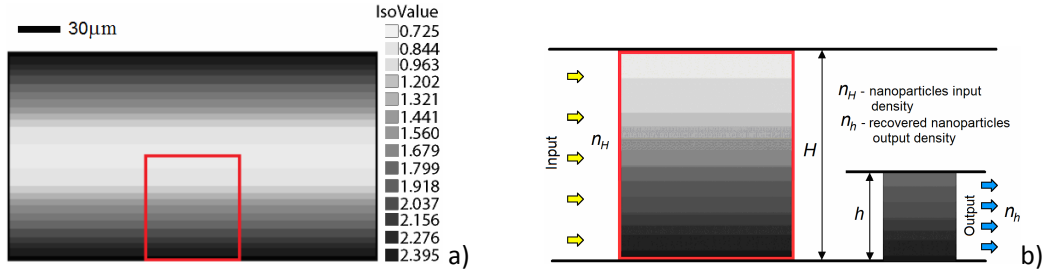


Figure 22: The calculated concentration field for suspended particles subjected to positive dielectrophoresis for $Q = 1$, a), and detail with the separation zone b).

One observes that the concentration field presents a layered structure, which allows an analytical description as a function of a single spatial variable, $C(y)$, where y is the vertical coordinate. Figure 22b shows a detail of Figure 22a with the delimited region of interest, having a height H and an arbitrary width. In this region, we considered the left hand part as the input zone of the nanoparticle and the right hand part as the nanoparticle output. From a practical point of view, it is obvious that if we are interested in the efficient recovery of the suspended particles, the process must take place in those regions of the fluid where the particle density is the highest. To obtain an efficient separation one must collect as many particles from the fluid suspension as possible, but at high values of particle concentration. In order to do this, a compromise value for the output width h ($0 \leq h \leq H$), is desirable: for a smaller h one separates a more concentrated fluid, while for a larger h one collects more particles, but at a lower concentration. As shown in Figure 23, the particle density at the output diminishes with h , and for small values of h it strongly depends on the intensity of the dielectrophoretic force Q .

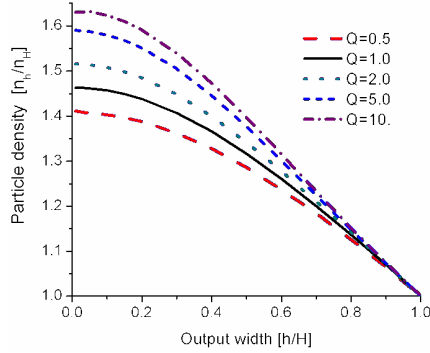


Figure 23: Calculated values for the output particle density, at different values for h and Q .

For the quantitative analysis of the separation process, we define the following set of parameters, related to the particles concentration distribution $C(y)$:

- the recovered mass at the output, named as *Recovery* (R):

$$R = \int_0^h C(y) dy \quad (12)$$

- the recovered nanoparticle output density:

$$n_h = (1/h) \int_0^h C(y) dy \quad (13)$$

- the quality of the separated fraction (i.e. the fraction of the separated nanoparticle concentration in the output) *Purity* (P):

$$P = \frac{n_h - n_0}{n_{\max} - n_0} \quad (14)$$

where $n_0 = 1$ is the value of the particle density in the absence of the dielectrophoretic force and n_{\max} is the particle density for $h \rightarrow 0$.

- the *Separation Efficiency* (SE) that provides more flexibility to evidence the efficiency at a certain stage of the separation, defined as:

$$SE = R + P - 1 \quad (15)$$

Next we discuss the importance of these parameters in the separation process of nanoparticles from flue gas in a microfluidic device based on dielectrophoresis.

Figure 24a shows the calculated values of *Recovery*, *Purity* and *Separation Efficiency* versus at various output widths h for a separation device having electrodes of $d=l=30\mu\text{m}$, and an applied voltage of $V_0=10\text{ V}$ on the electrodes. The computations were performed for three different values of particle radius, $a=50\text{nm}$, 100nm and 150 nm . Figure 24b is a detail revealing the optimal values for separation: the intersections for *RP* and the maxima for *SE*.

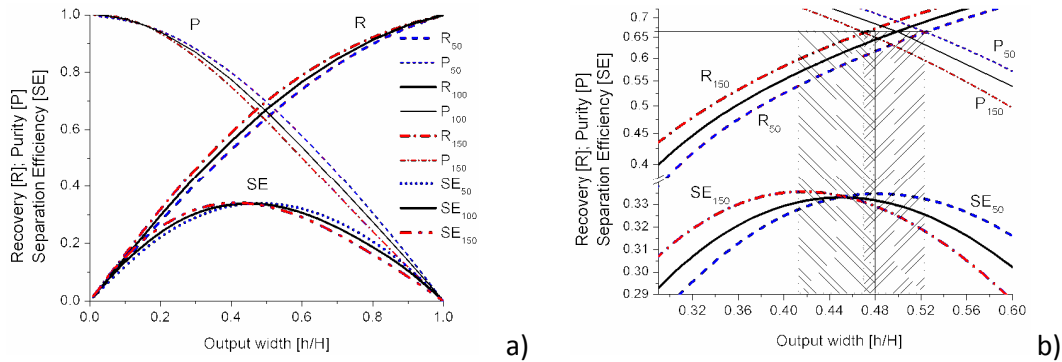


Figure 24: *Recovery*, *Purity* and *Separation Efficiency* as function of the collector height h , for the radius values: $a=50$, 100 , 150 nm , a), detail b). The subscripts in the legend and on graphs denote the particle radii.

One observes that in all cases *Separation Efficiency* first increases when increasing the output width h , achieves a maximum approximately at the intersection of *Recovery* – *Purity* plots, and then decreases with h . One notices a quite low influence of the particle size on the separation efficiency. With increasing h , the amount of particles remained in the output (recovered mass or product – R) increases too, while *Purity* decreases. $P=1$ corresponds to the maximum value of the particle concentration in the product, and $R=1$ corresponds to the case when all the material ends up in the product. Therefore, a compromise must be found between the purity of the product, which will set the amount of the product. A reasonable choice for this compromise value is the maximum of *SE* curve. According to the presented separation diagram, the maximum separation accuracy is obtained at intermediate values of the ratio h/H between 0.41 and 0.48 (the shaded area in the left, between the maximum leftmost and rightmost values of *SE*, corresponding to $a=50\text{nm}$ and $a=150\text{nm}$). On the other hand, taking into account the leftmost and rightmost R – P intersections (the shaded area in the right, corresponding also to $a=50\text{nm}$ and $a=150\text{nm}$), one obtains for h/H values ranging from 0.47 to 0.53. For values of h/H in the domain 0.47–0.48 (the double shaded zone in the middle, obtained by intersection between the left – right shaded zones), one obtains the optimum separation mode, for which one achieves the values $R\sim P\sim 0.67$, corresponding to the discussed compromise.

- The influence of problem parameters on the particle trajectories

In this study, we performed a numerical analysis regarding the influence of the main parameters, which act on the particles trajectories, when subjected to *travelling* DEP force. The trajectories were computed by integrating the movement equation $\mathbf{x} = \mathbf{x}_0 + \mathbf{v}_0 t + 1/2 \mathbf{a} t^2$ using the *tw*DEP force given by (10). The flow was considered laminar, described by a Poiseuille type profile, having the maximum value for the flow velocity inside the channel $10\ \mu\text{m/s}$, the characteristic length of the device being $d = 50\mu\text{m}$. Figure 25 presents a set of relevant numerical results regarding the influence of this parameters on the trajectories.

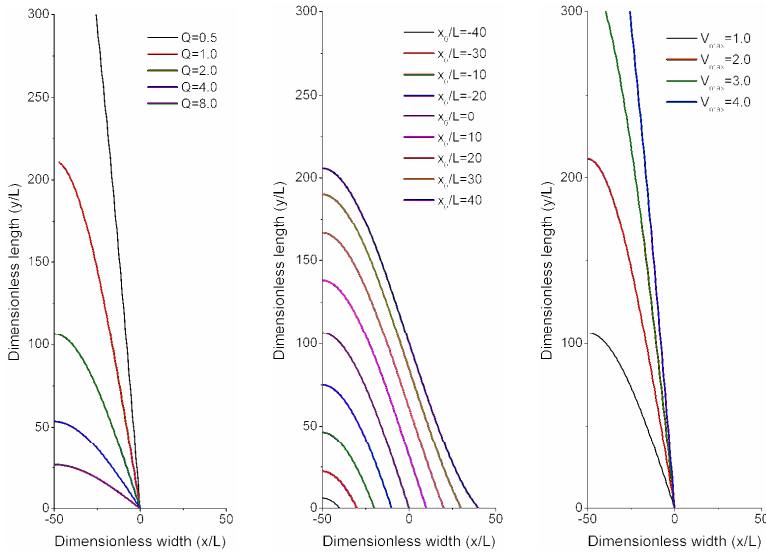


Figure 25: The influence of the main parameters on the particle trajectory when subjected to $twDEP$ force.

- **The analysis of the dielectric behaviour of particles from burning ash (the frequency dependence of the complex permittivity and of the Clausius Mossotti factor for the analyzed particles).**

At this stage of the project we performed a preliminary study on the possibility to capture nanoparticles from flue gas by using dielectrophoresis, in order to improve the filtration process. The test probe is a powder sampled from the filters of the Pro Air Clean Timisoara waste incinerator.

The analysis consisted of the measurement of the Clausius- Mossotti (CM) factor in low frequency filed (25 Hz-2MHz). The measurement of the real and imaginary parts of the complex dielectric permittivity were performed with a Agilent type RLC-meter(E4980A), to which a cylindrical capacitor, containing the probe, was connected. The capacity C and the quality factor Q were measured, at constant temperature and for the desired frequency domain, with, (C_p, Q_p) , and without probe, (C_0, Q_0) .

The components ϵ' and ϵ'' of the complex dielectric permittivity were calculated using the following relations [19]:

$$\epsilon' = \frac{C_p}{C_0} ; \epsilon'' = \frac{Q_0 C_p - Q_p C_0}{Q_p Q_0 C_0} . \quad (16)$$

The analyzed probe is a mixture of micro and nanoparticles dispersed in air. In this case, the complex dielectric permittivity of the mixture is obtained by using the relation:

$$\tilde{\epsilon}_{eff} = \epsilon'_{eff} - i\epsilon''_{eff} \quad (17)$$

In equation (17) ϵ'_{eff} and ϵ''_{eff} , are the real and the imaginary parts of the complex dielectric permittivity $\tilde{\epsilon}_{eff}$, and depend on the frequency. The frequency dependence for different volume fractions of the particle mixture is presented in Figure 26.

One can observe from Figure 26a that for each volume fraction Φ , the real part of the effective dielectric permittivity ϵ'_{eff} , decreases with frequency, from the approximate value 1.8 to the approximate value 1.2. The imaginary component of the effective complex dielectric permittivity, ϵ''_{eff} decreases with frequency for each constant volume fraction Φ , from the large values to approximately zero (Figure 26b). The large values of ϵ''_{eff} at the beginning of the measurement frequency range, are an indication of high conduction losses of the sample (see Figure 26b), this fact being in accordance with the EDAX analysis (see Figure 31b)), which indicates a high content (the atomic fraction more than 68%) of carbon in the investigated sample.

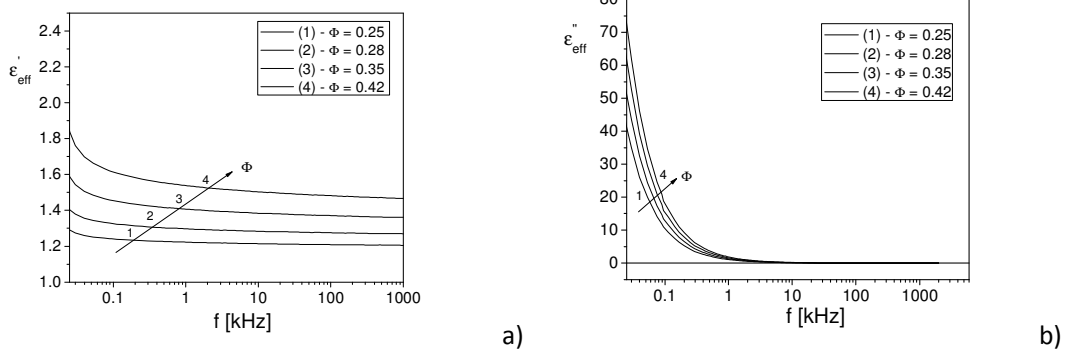


Figure 26: The frequency dependence of the real ϵ'_{eff} , and imaginary ϵ''_{eff} components of the complex dielectric permittivity $\tilde{\epsilon}_{eff}$ at different volumic fraction Φ of the particles.

Also, over the entire frequency range, both ϵ'_{eff} and ϵ''_{eff} , increase with volume fraction Φ , for a constant frequency. For the effective dielectric constant of the composite systems, there have been developed many approaches involving theoretical and experimental studies. The volume-fraction average model [19] is a simple method estimating the effective dielectric constant, of a mixture/composite system containing two phases:

$$\epsilon_{eff} = (1-\Phi)\epsilon_m + \Phi\epsilon_p \quad (18)$$

where Φ is the volume fraction of the particles from mixture.

For the investigated ash powder sample dispersed in air, using the complex form, the dielectric constants in equation (9), the real ϵ'_p and the imaginary ϵ''_p , components of the particle, were computed with equation (10). The dispersion medium being the air, we have used in equation (9) the following values for the components of complex dielectric permittivity: $\epsilon'_m(air) = 1$ and $\epsilon''_m(air) = 0$. We obtain:

$$\epsilon'_p = \frac{\epsilon'_{eff} - 1 + \Phi}{\Phi}, \quad \epsilon''_p = \frac{\epsilon''_{eff}}{\Phi}, \quad (19)$$

The frequency dependence of the ϵ'_p and ϵ''_p components of the effective complex dielectric permittivity of the ash particles, computed with equations (10), for different volume fractions Φ , are presented in Figure 27.

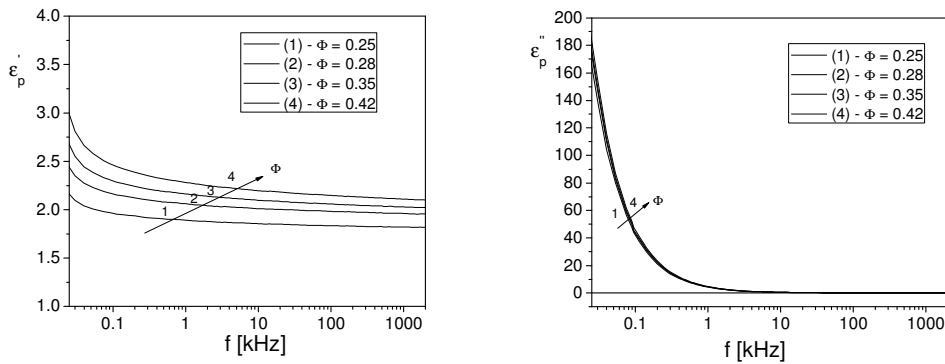


Figure 27: The frequency dependence of the real (ϵ'_p) and imaginary (ϵ''_p) components of the complex dielectric permittivity for ash particles dispersed in air, at different volumic fractions Φ .

One can observe from Figure 27a that for each volume fraction Φ , the real part of the ash particle dielectric permittivity ϵ'_p , decreases with frequency, from the approximate value 3 to the approximate

value 2. The imaginary component of the dielectric permittivity ash particle ϵ_p'' , has approximately the same value for all volume fractions Φ , and decreases with frequency, from the large values to approximate zero (Figure 27b). The large values of ϵ_p'' from the beginning of the measurement frequency range, are an indication of the high conduction losses in sample (see Figure 27b), this fact being in accordance with the frequency dependence of the imaginary component ϵ_{eff}'' , of the effective dielectric permittivity (see Figure 27b).

By introducing in equations (5) and (6) the calculated values for ϵ_p' and ϵ_p'' (Figure 27), and considering that the dispersion medium is the air (with $\epsilon_{air}' = 1$ and $\epsilon_{air}'' = 0$), we can determine the real part, $\text{Re}[\tilde{K}(\omega)]$ and imaginary part, $\text{Im}[\tilde{K}(\omega)]$ of the Clausius-Mossotti complex factor. The frequency dependence of the $\text{Re}[\tilde{K}(\omega)]$ and $\text{Im}[\tilde{K}(\omega)]$ parts of the CM factor is shown in Figure 28.

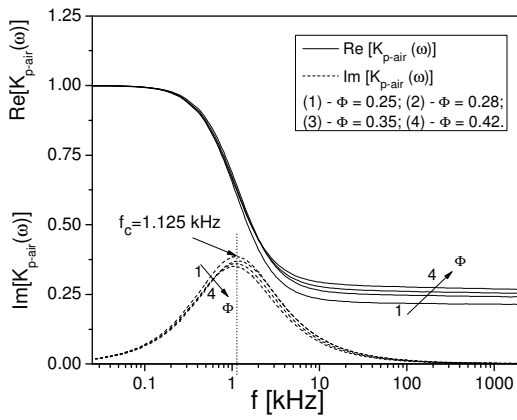


Figure 28: Frequency dependence of the real $\text{Re}[\tilde{K}_{p-air}(\omega)]$ and imaginary $\text{Im}[\tilde{K}_{p-air}(\omega)]$ components of the complex Clausius-Mossotti factor for different volumic fractions Φ of the particles dispersed in air.

As seen in Figure 28, the frequency dependence of the real and imaginary components of the CM factor fits with a Debye type dependence. The real part of CM factor ($\text{Re}[\tilde{K}_{p-air}(\omega)]$), for all investigated frequency range is positive. Therefore, dielectrophoresis is positive (pDEP) and, in this case it can do a filtering of flue gas using pDEP, by trapping the nanoparticle in the area of the strongest electric field. The imaginary component of the CM factor, $\text{Im}[\tilde{K}_{p-air}(\omega)]$ presents a maximum at the same frequency, $f_c = 1.125 \text{ kHz}$, regardless of the volume fraction Φ , of ash particles dispersed in air. The associated peak of the imaginary component, at the frequency f_c , (Figure 28), is correlated with the relaxation time, τ_{MW} , by the Debye relation, $2\pi f_c \tau_{MW} = 1$, The value obtained for the relaxation time is $\tau_{MW} = 0.1414 \text{ ms}$ and this relaxation time is called dipolar Maxwell-Wagner relaxation time, being typical for the particles with dielectric and conduction losses [19].

Because the CM factor represents a measure of the relative permittivity between the particle and the surrounding medium, the real component, $\text{Re}[\tilde{K}(\omega)]$ determines the sign of the DEP force.

We have theoretically analyzed the sign of the real component of CM factor when the ash particles are dispersed in a medium without loss, whose dielectric permittivity ϵ_m , varies from 3 to 10. We have determined in both cases, the real $\text{Re}[\tilde{K}_{p-m}(\omega)]$ and imaginary $\text{Im}[\tilde{K}_{p-m}(\omega)]$ components of the Clausius-Mossotti factor in equations (18) and (19) using the calculated values of ϵ_p' and ϵ_p'' (Figure 27), and considering two cases for the surrounding medium: 1) $\epsilon_{m,1}' = 3$ and $\epsilon_{m,1}'' = 0$; 2) $\epsilon_{m,2}' = 10$ and $\epsilon_{m,2}'' = 0$.

In this case, the relations for $\text{Re}[\tilde{K}_{p-m}(\omega)]$ and $\text{Im}[\tilde{K}_{p-m}(\omega)]$ are:

$$\operatorname{Re}[\tilde{K}(\omega)] = \frac{\varepsilon_p'^2 + \varepsilon_p''^2 + \varepsilon_p' \varepsilon_m' - 2\varepsilon_m'^2}{\varepsilon_p'^2 + \varepsilon_p''^2 + 4\varepsilon_p' \varepsilon_m' + 4\varepsilon_m'^2} \quad (20)$$

$$\operatorname{Im}[\tilde{K}(\omega)] = \frac{3\varepsilon_p'' \varepsilon_m'}{\varepsilon_p'^2 + \varepsilon_p''^2 + 4\varepsilon_p' \varepsilon_m' + 4\varepsilon_m'^2} \quad (21)$$

Figure 29 shows the frequency dependence of these components, for two values of the volume fraction of the ash particles dispersed in a fluid medium ($\Phi = 0.25$ and $\Phi = 0.42$).

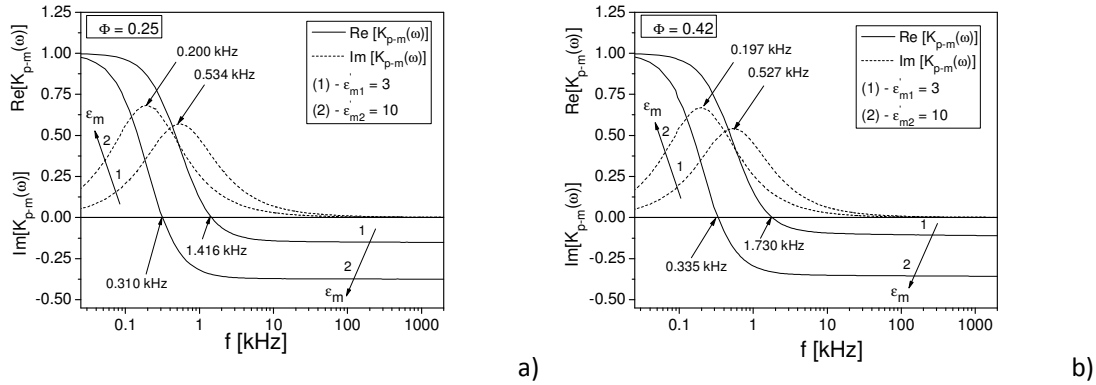


Figure 29: Frequency dependence of the real $\operatorname{Re}[\tilde{K}_{p-m}(\omega)]$ and imaginary $\operatorname{Im}[\tilde{K}_{p-m}(\omega)]$ components of the complex Clausius-Mossotti factor for two values of the volumic fraction, $\Phi = 0.25$ (a) and $\Phi = 0.42$ (b), for particles dispersed in fluids with $\varepsilon_m = [3,10]$.

As seen in Figure 29, the real component $\operatorname{Re}[\tilde{K}_{p-m}(\omega)]$, of the CM factor changes its sign, from positives values to negatives values for both analyzed volume fractions of the ash particles dispersed in any fluid medium having a dielectric permittivity $\varepsilon_m = [3,10]$. The sign change occurs at a critical frequency f_c , which decreases from 1.416 kHz to 0.31 kHz (for $\Phi = 0.25$) and from 1.730 kHz to 0.335 kHz (for $\Phi = 0.42$), if the dielectric permittivity of the medium increases from 3 to 10. Therefore, there is a shift from positive dielectrophoresis (pDEP) to negative dielectrophoresis (nDEP), and the particles can move from regions of high electric field gradient to regions of low electric field gradient. This result shows that it is possible to use dielectrophoresis in order to obtain a selective separation of nanoparticles, depending on the frequency of the electric field, on the dispersion medium and the physical properties of ash nanoparticles. If the ash particles are dispersed in air, $\operatorname{Re}[\tilde{K}_{p-air}(\omega)] > 0$ for all the investigated frequency domain. Consequently, it is possible to filtrate the flue gas by using the positive dielectrophoresis by attracting the particles in the regions with high electric field (on the margins of the electrodes).

6. Experimental researches and modeling on manipulation of nanoparticles in flue gas fluid suspensions subject to non uniform electric fields (dielectrophoresis), based on simulations results.

Activities:

- **Chemical and size classes analysis of the particles, exhausted by incinerator of ProAirClean Timisoara, especially using LM10 Nanosight microscope, acquired in the 2012 project phase. Comparison of the obtained results with data from literature.**

The analysed probes consist of 4 representative samples, prelevated from the burning ashes collected from the filters of Pro Air Clean Timisoara incinerator, during a 6 month period (June-November 2013).

The goals were as follows:

- The determination of the chemical composition using the existing equipment at Pro Air Clean Timisoara

Table 1 presents the AAS analysis for the ash probes, performed with the KONTRAA 700 spectrophotometer, which reveals the metallic and organic carbon (TOC) content of the probes. For

example, the important Al content (16,64%) in probe 1 determines a high conductivity of the probe, and supports the hypothesis that the high value of the CM factor appears at low frequencies.

Table 1: Metallic content of the ash probes

| Chemical elements | Content | | | | | | | |
|-------------------|---------|--------------|---------|--------------|---------|--------------|---------|--------------|
| | Probe 1 | | Probe 2 | | Probe 3 | | Probe 4 | |
| | mg/kg | % | mg/kg | % | Mg/kg | % | Mg/kg | % |
| Al | 166440 | 16,64 | 3890 | 0,39 | 3480 | 0,35 | 44890 | 4,5 |
| Cd | 328 | 0,033 | 198 | 0,02 | 198 | 0,02 | 248 | 0,025 |
| Co | 100 | 0,01 | 122 | 0,012 | 122 | 0,012 | 99 | 0,01 |
| Cr | 110 | 0,01 | 98 | 0,01 | 98 | 0,01 | 105 | 0,01 |
| Cu | 1450 | 0,145 | 4490 | 0,45 | 4490 | 0,45 | 4230 | 0,42 |
| Fe | 39670 | 3,97 | 13980 | 1,4 | 34980 | 3,5 | 56970 | 5,7 |
| Mn | 5390 | 0,54 | 148 | 0,15 | 159 | 0,16 | 890 | 0,09 |
| Ni | 500 | 0,05 | 390 | 0,04 | 190 | 0,02 | 328 | 0,033 |
| Pb | 9870 | 0,99 | 510 | 0,05 | 970 | 0,1 | 700 | 0,07 |
| Sb | 140 | 0,014 | 108 | 0,01 | 98 | 0,01 | 100 | 0,01 |
| Zn | 48760 | 4,88 | 17980 | 1,8 | 78980 | 7,9 | 5390 | 0,54 |
| TOC ¹ | 31980 | 3.2 | 27870 | 2.8 | 23950 | 2.4 | 39980 | 4.0 |

- *Dimensional analysis with the Nanosight LM 10 microscope, aquired in the 2012 phase of the projecti*

For the dimensional measurements were prepared, for each of the four ash probes, a mixture of 5 mg of powder and 100 ml of distilled water at room temperature, letting the mixture to decantation (to eliminate the microparticles) 20 minutes for the first measurement and 10 more minutes for the second measurements. In each case, after the decantation of microparticles, the remaining liquid was collected and analyzed from a size/concentration distribution point of view using the nanoparticle visualization system Nano Sight LM10. This equipment determines the size distribution of nanoparticles in polidisperse and heterogeneous systems, using the Nanoparticle Tracking Analysys (NTA) method.

Probe 1

Figure 30a presents a video frame, and Figure 30b reveals the size/concentration distribution of nanoparticles in probe 1, after 20 minutes decantation time, according to the analysis report generated by the nanoscope LM 10 software. The distribution diagram indicates that there exist four relevant particle radii, having values of 55 nm, 100 nm, 155 nm and 275 nm, respectively.

For the next three probes we performed two measurements for each, after 20 minutes and 30 minutes decantation time, respectively.

Figures 31 presents the X ray diffraction spectrum (a) and the composition of probe 1 determined by EDAX analysis (b). The EDAX analysis indicates a high level of inorganic carbon, as expected. Wt (%) is the mass fraction and A_t (%) is the atomic fraction, in percents.

¹ For the correct functioning of the incinerator, the TOC concentration must not exceed 4%.

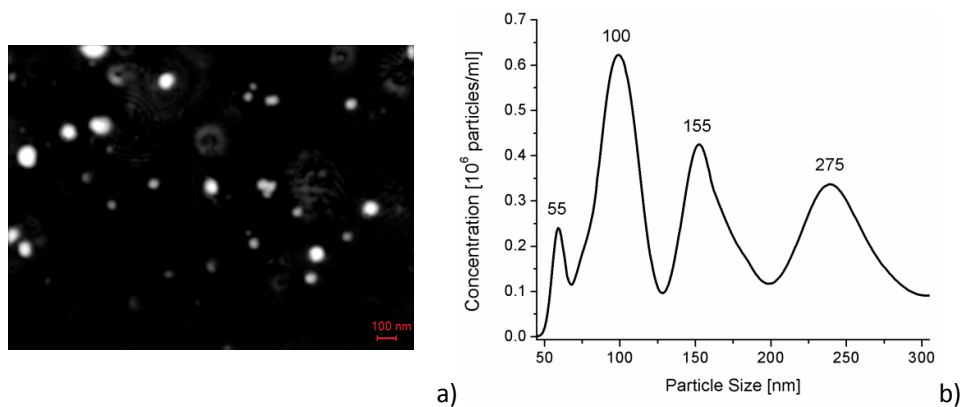


Figure 30: Video frame from the analysis report a) and size/concentration distribution for probe 1, obtained by nanoparticle visualisation system Nano Sight LM10, after 20 minutes decantation time.

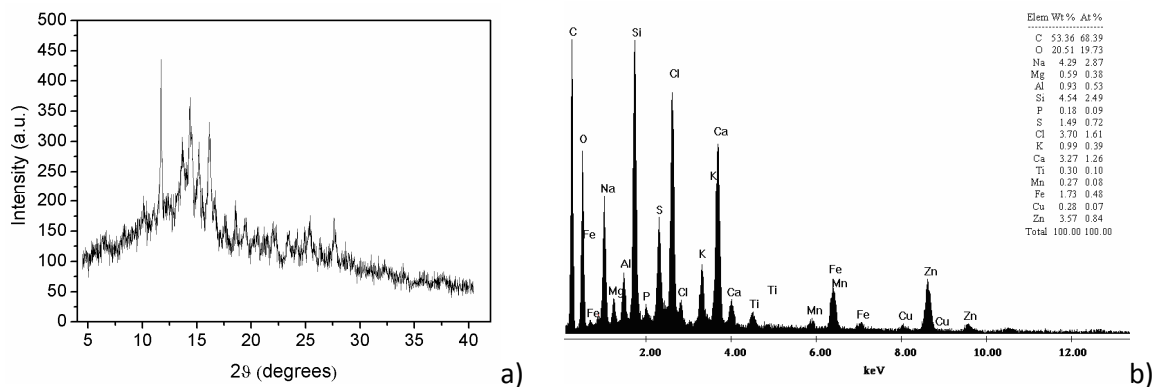


Figure 31: X ray diffracton spectrum for investigated ash a), and EDAX analysis b)

Probe 2

Figure 32a presents the size/concentration distribution of nanoparticles for the probe 2, after 20 minutes decantation time. The distribution diagram indicates that there exist five relevant particle radii, having values of 70 nm, 115 nm, 148 nm, 189 nm and 266 nm, respectively. Figure 32b illustrates the size/concentration distribution of nanoparticles for probe 2, after 10 more minutes of decantation time. The distribution diagram indicates that there exist three relevant particle radii, having values of 45 nm, 93 nm and 154 nm, respectively.

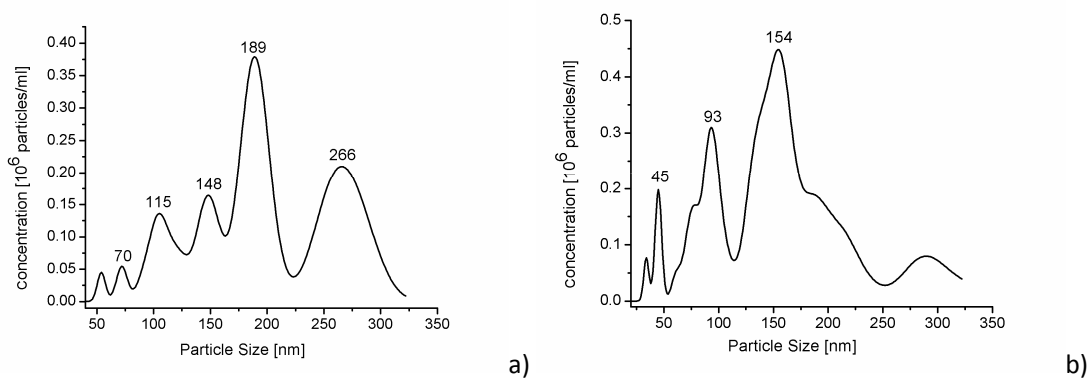


Figure 32: Size/concentration distribution for probe 2, obtained by nanoparticle visualisation system Nano Sight LM10, after 20 minutes decantation time a), and after 30 minutes decantation time b).

Probe 3

Figure 33a presents the size/concentration distribution of nanoparticles for the probe 3, after 20 minutes decantation time. The distribution diagram indicates that there exist four relevant particle radii, having values of 44 nm, 67 nm, 109 nm and 180nm, respectively. Figure 33b illustrates the size/concentration

distribution of nanoparticles for probe 3, after 10 more minutes of decantation time. The distribution diagram indicates that there exist three relevant particle radii, having values of 37 nm, 56 nm and 95 nm, respectively.

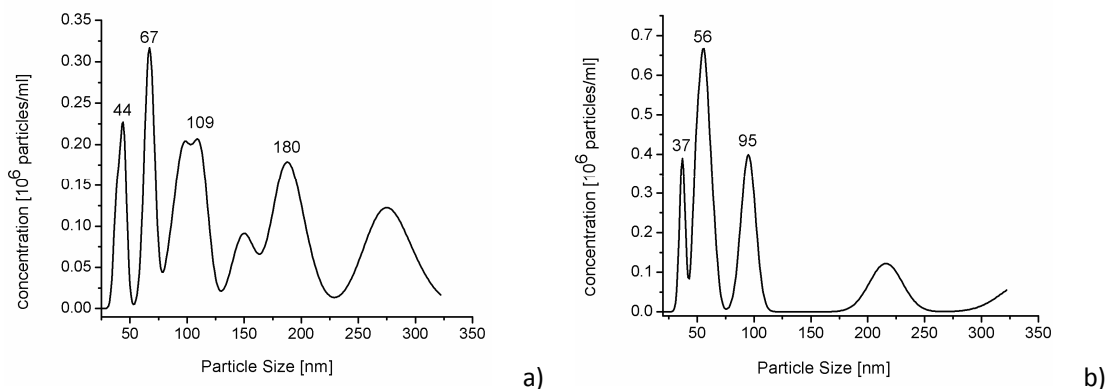


Figure 33: Size/concentration distribution for probe 3, obtained by nanoparticle visualisation system Nano Sight LM10, after 20 minutes decantation time a), and after 30 minutes decantation time b).

Probe 4

Figure 34a presents the size/concentration distribution of nanoparticles for the probe 4, after 20 minutes decantation time. The distribution diagram indicates that there exist five relevant particle radii, having values of 40 nm, 60 nm, 102 nm, 138 nm and 175 nm, respectively. Figure 34b illustrates the size/concentration distribution of nanoparticles for probe 4, after 10 more minutes of decantation time. There exist three relevant particle radii, having values of 42 nm, 95 nm and 175 nm, respectively.

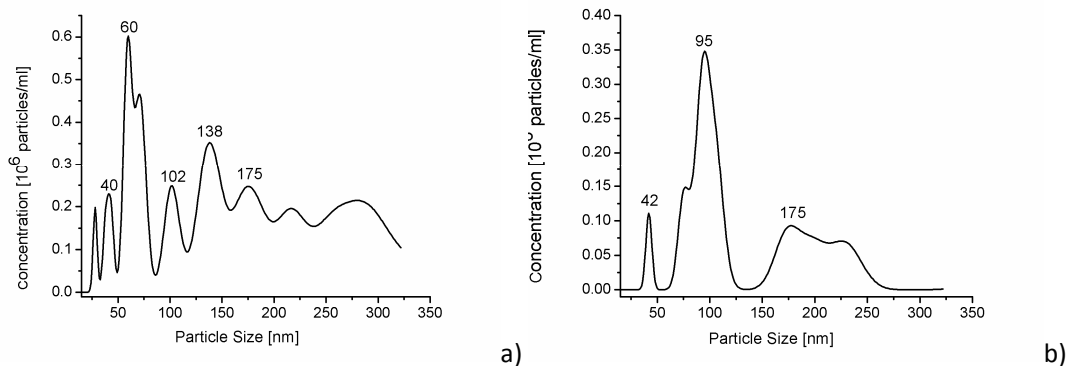


Figure 34: Size/concentration distribution for probe 4, obtained by nanoparticle visualisation system Nano Sight LM10, after 20 minutes decantation time a), and after 30 minutes decantation time b).

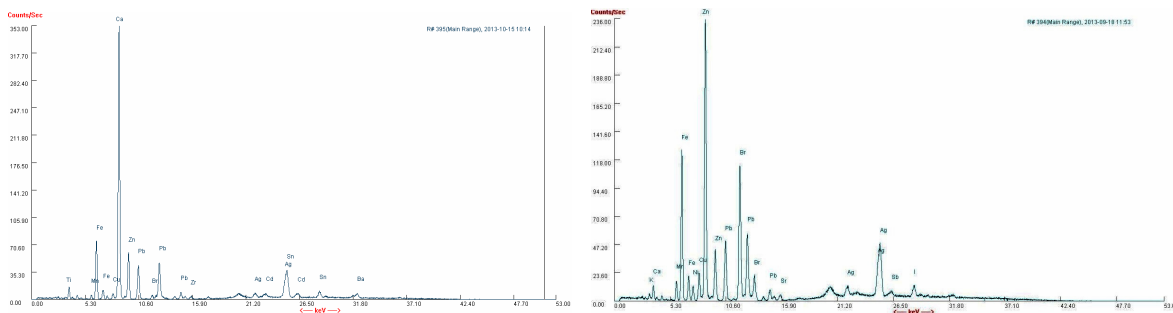


Figure 35: The metallic content of the particles in probes 3 and 4, obtained by X ray analysis. In probe 3 prevails Ca, while in probe 4 prevails Zn.

- The design and build-up of an experimental device for retaining the nanoparticles from combustion gases in non-uniform electric fields.

Based on the results obtained by simulations, an experimental device was designed and is being under development in collaboration with Pro Air Clean Timisoara and the Faculty of Physics from University of Bucharest, for retaining nanoparticles from flue gas in nonuniform electric field. The bottom and upper parts of the microfluidic separation device sketched in Figure 9 are presented in Figure 36a, while the corresponding Gerber diagram (the layout at micrometric scale), required to obtain the experimental device by metallic evaporation and vacuum deposition on an insulating plate, performed at the University of Offenburg Germania, is shown in Figure 36b.

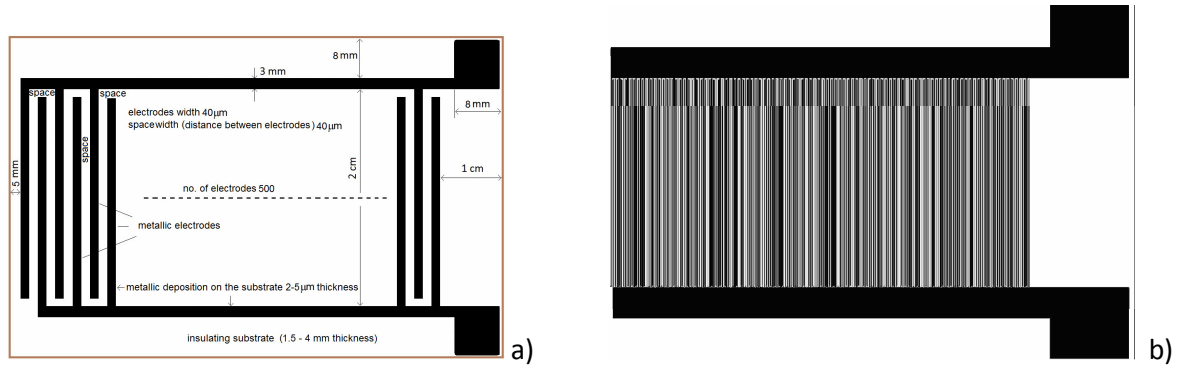


Figure 36: Schematic representation of the bottom and upper parts of the microfluidic separation device a), the Gerber diagram representing the layout at micrometric scale b).

The group coordinated by Prof. Dr. Stefan Antohe from the Faculty of Physics de la Facultatea de Fizica, University of Bucharest, obtained test subassemblies for the experimental device, consisting of Cu electrodes with a purity of 99.99% deposited in vacuum on Fisher glass plates, in different geometries (interdigitated and simple) as shown in Figure 35.

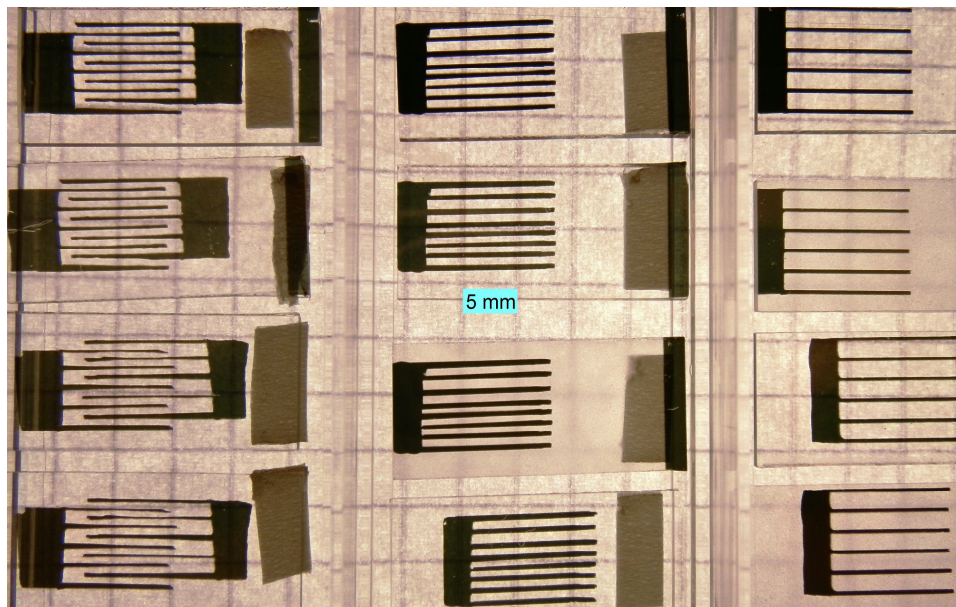


Figure 37: Different subassemblies of the experimental device for the capture of nanoparticles suspended in gas flue – electrodes of 99.99% purity Cu, deposited in vacuum on Fisher glass plates.

Conclusions

The numerical results obtained in the frame of the proposed mathematical model reveals the role of the main parameters (the nature and the dimension of the particles, the geometry of the device, the flow velocity, the applied voltage, the geometry of the electrodes) on particle manipulation for separation and flue gas purification. The results show the possibility to filtrate flue gas by dielectrophoresis and

demonstrate that the filtration process efficiency can be improved based on the mathematical modelisation and simulations.

The chemical analysis demonstrated the presence of numerous metals in burning ashes, metals which, once liberated in the atmosphere as nanoparticles have an important negative impact on human health. Also, the organic and inorganic carbon presents an important risk for the environment when presented as nanoparticles.

The dimensional analysis show that the flue gases resulted after the waste burning contain nanoparticles. The observed nanoparticles are those which probably remained attached to larger particles, stocked during the mechanical filtration process, but they are still relevant for our study, because they indicate the existence of much more nanoparticle in the flue gases. The presented study focused mainly on particles with radii <200 nm, which are potentially harmful for the human health.

Finally, a set of test subassemblies for the experimental device were obtained together with the group coordinated by Prof. Dr. Stefan Antohe from the Faculty of Physics, University of Bucharest, consisting of electrodes of 99.99% purity Cu, deposited in vacuum on Fisher glass plates in different geometries (interdigitated and simple).

7. Dissemination of the obtained results.

The results obtained in the first three stages (2011 -- 2013) were disseminated in the frame of international conference and papers published or submitted for publication in ISI journals as in the list below, used also for references. During the stage the project website was constantly updated, at the address: www.nanodep.com.

Conference participations:

- [1] A. Neculae, M. Lungu, M. Bunoiu, R. Giugiulan: Electrohydro-dynamic modeling for manipulation of micro/nano particles in microfluidic systems; Physics Conference TIM 11, Timisoara, Romania, November 24-27, 2011.
- [2] M. Lungu, A. Neculae, M. Bunoiu, N. Strambeanu, R. Giugiulan: Reduction of nanoparticle emission by electrohydrodynamic filtering of residual combustion gases; International Conference ANMBES 2012. Transilvania University of Brasov, Romania, May 24th-27th, 2012, Abstract Book p.107.
- [3] M. Lungu, I. Malaescu, R. Giugiulan, M. Bunoiu and N. Strambeanu: Experimental investigations on the frequency dependence of the Clausius-Mossotti factor for nano/ microparticles contained in the exhausted flue gases of incinerators, the 8th General Conference of Balkan Physical Union, Constanta, Romania, July 5-7, 2012, Abstract Book p.155.
- [4] M. Lungu, A. Neculae, R. Giugiulan, M. Bunoiu and A. Lungu: Effects of flow velocity upon nanoparticle distribution in microfluidic devices under dielectrophoresis; ICPAM-9, 9th International Conference on Physics of Advanced Materials, Iasi, Romania, 20-23 September 2012, Abstract Book p.105.
- [5] A. Neculae, R. Giugiulan and M. Lungu: Nanoparticle manipulation by dielectrophoresis, IX Conference of the Society of Physicists of Macedonia, Ohrid, Republic of Macedonia, 20-23 September 2012.
- [6] M. Lungu, A. Neculae, M. Bunoiu, R. Giugiulan: Separation of submicron particles suspended in fluid wastes using dielectrophoresis; The Proceedings of XIII-th International Mineral Processing Symposium, Bodrum, Turkey, October 10 - 12, 2012, p.865-870.
- [7] A. Neculae, R. Giugiulan, M. Bunoiu M. Lungu: Submicron particle trapping using traveling wave dielectrophoresis; TIM-12 Physics Conference, Timisoara, Romania, November 27-30, 2012.
- [8] Malaescu, C.N. Marin, S. Satulu: The temperature and particle concentration influence on the complex dielectric permittivity of magnetic fluids; TIM-12 Physics Conference, Timisoara, November 27-30, 2012, Abstract Book p.118.
- [9] A. Neculae, R. Giugiulan, M. Lungu and N. Strambeanu: Separation of nanoparticles from combustion gases wastes of incinerators; IMCET 2013, The 23-rd International Mining Congress and Exhibition of Turkey, Kemer-Antalya, Turcia, 16-19 April 2013.
- [10] A. Neculae, M. Bunoiu, T. Marian and M. Lungu: 3D Numerical analysis of nanoparticle suspension distribution in a microfluidic device under dielectrophoresis; The 13th International Balkan Workshop on Applied Physics, Constanta, July 4-6, 2013.
- [11] I. Malaescu, R. Giugiulan, M. Lungu and N. Strambeanu: The Clausius-Mossotti factor in low frequency field of the powders resulted from waste combustion; The 13th International Balkan Workshop on Applied Physics, Constanta, July 4-6, 2013.
- [12] M. Lungu, R. Giugiulan, M. Bunoiu and A. Neculae: Symulation study of a 3D DEP-based microfluidic system; TIM-13 Physics Conference, Timisoara, Romania, November 21-24, 2013.

ISI Publications:

- [13] M. Lungu, A. Neculae, M. Bunoiu, N. Strambeanu: Some considerations on the nanoparticles manipulation in fluid media using dielectrophoresis; *Romanian Journal of Physics*, Vol. 56 (5-6), p. 749-756, 2011.
- [14] A. Neculae, M. Lungu, M. Bunoiu, R. Giugiulan: Electrohydro-dynamic modeling for manipulation of micro/nano particles in microfluidic systems; *American Institute of Physics Conference Proceedings* 1472, Proceedings of the physics conference TIM-11, Melville, New York, 2012, p. 155-161.
- [15] A. Neculae, M. Lungu, C.G. Biris, M. Bunoiu: *Numerical analysis of nanoparticles behavior in a microfluidic channel under dielectrophoresis*, Journal of Nanoparticle Research, Volume: 14, Issue: 1154, p.1-12, 2012.
- [16] M. Lungu, A. Neculae, M. Bunoiu, R. Giugiulan: *Separation of submicron particles suspended in fluid wastes using dielectrophoresis*; The Proceedings of XIII-th International Mineral Processing Symposium, Bodrum, Turkey, October 10 - 12, 2012, p.865-870.
- [17] A. Neculae, R. Giugiulan and M. Lungu: Nanoparticle manipulation by dielectrophoresis; *Physica Macedonica*, ISSN 1409-7168, vol 61, p. 39-44, 2012.
- [18] A. Neculae, R. Giugiulan, M. Bunoiu and M. Lungu: Effects of flow velocity upon nanoparticle distribution in microfluidic devices under dielectrophoresis, *Romanian Reports in Physics*, vol. 2, 2014 (in press).
- [19] I. Malaescu, M. Lungu, R. Giugiulan and N. Strambeanu: The Clausius-Mossotti factor in low frequency field of the powders resulted from waste combustion, *Romanian Journal of Physics* 2013 (in press).
- [20] A. Neculae, R. Giugiulan, M. Bunoiu, M. Lungu: Submicron particle trapping using traveling wave dielectrophoresis; *American Institute of Physics Conference Proceedings*, Proceedings of the physics conference TIM-12, Melville, New York, 2013 (in press).

Stage 2014 (December 16, 2013 – December 15, 2014)

Main objectives:

8. Performing experiments on nanoparticle trapping from flue gases resulting from waste incinerator Pro Air Clean Timisoara, by using the experimental device.

Based on the results obtained from the mathematical models and numerical simulations performed at earlier stages, and on the design from the stage 2013, was realized and tested a laboratory microfluidic device for retaining nanometric particles in non-uniform electric field by positive dielectrophoresis (pDEP). Practical tests were conducted on emission source represented by a pilot plant for incineration, by burning of waste categories specific to the Clean Air Pro Timisoara incinerator. The main active parts of the device consist in the deposition plates, made by PCB (Printed Circuit Board) technique at the University of Offenburg, Germany, Figure 1), based on the Gerber diagram performed in Sage 2013 (Figure 1d), with electrode width and gap between electrodes $d = l = 100\mu\text{m}$.

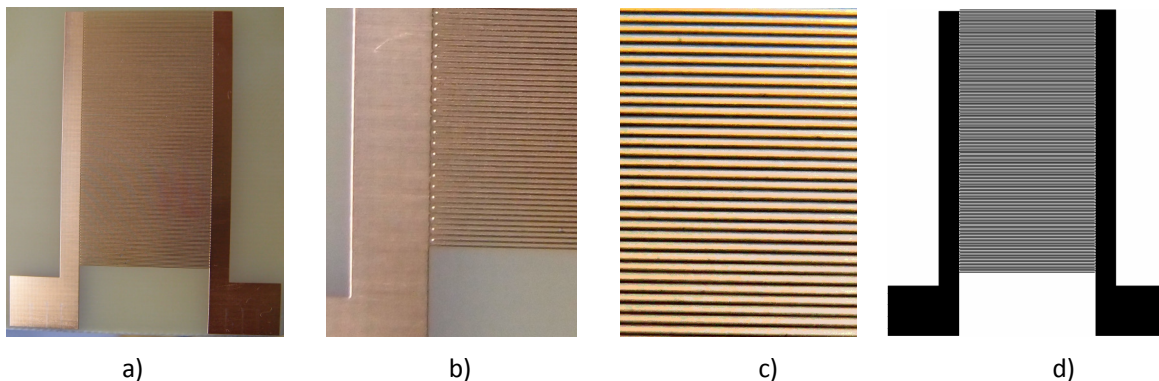


Figure 1: Deposition plate made by PCB (Printed Circuit Board) technique, a), detail of interdigitated electrodes, b), magnified image (10x) of the electrodes, c), Gerber diagram, d).

Activities:

- Analysis and characterization of the collected particles.

Nanoparticles collected from flue gas by positive dielectrophoresis on the deposition plates of the experimental microfluidic device with interdigitated parallel electrodes placed on an insulating substrate, schematically represented in Figure 2, were dimensionally, chemically and morphostructurally analyzed and characterized.

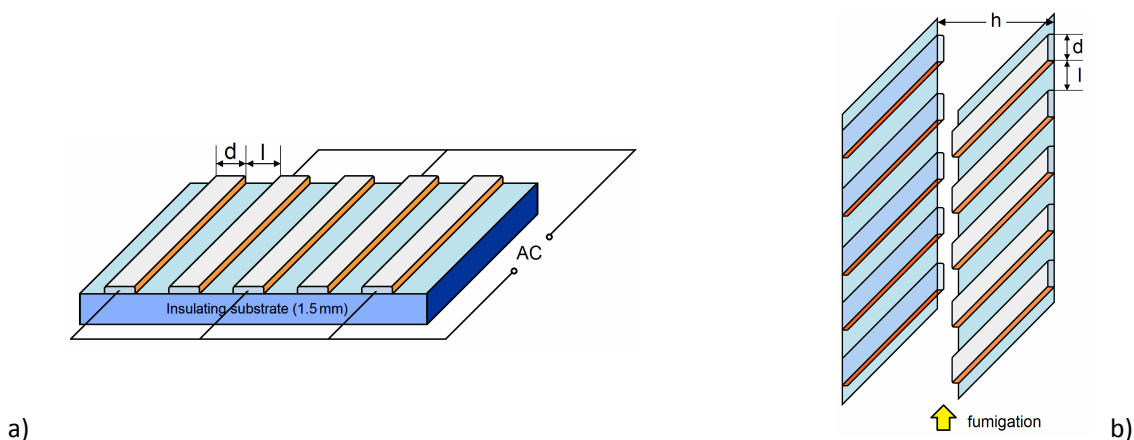


Figure 2: Detail of experimental microfluidic device with interdigitated parallel electrodes placed on an insulating substrate, a), schematic representation of the experimental device used to retain nanoparticles from flue gas based on pDEP placed in working position, b). Electrode width and gap between electrodes $d = l = 100\mu\text{m}$, distance between deposition plates $h=2\text{ mm}$.

Practically, we conducted experiments to capture the nanoparticles from flue gas by introducing them at the bottom part of the test device. The installation is shown in Figure 3a), with detail of the pilot plant

for combustion of specific wastes in Figure 3b) below, and detailed experimental device with entering of the flue gases at the bottom part in Figure 3c).

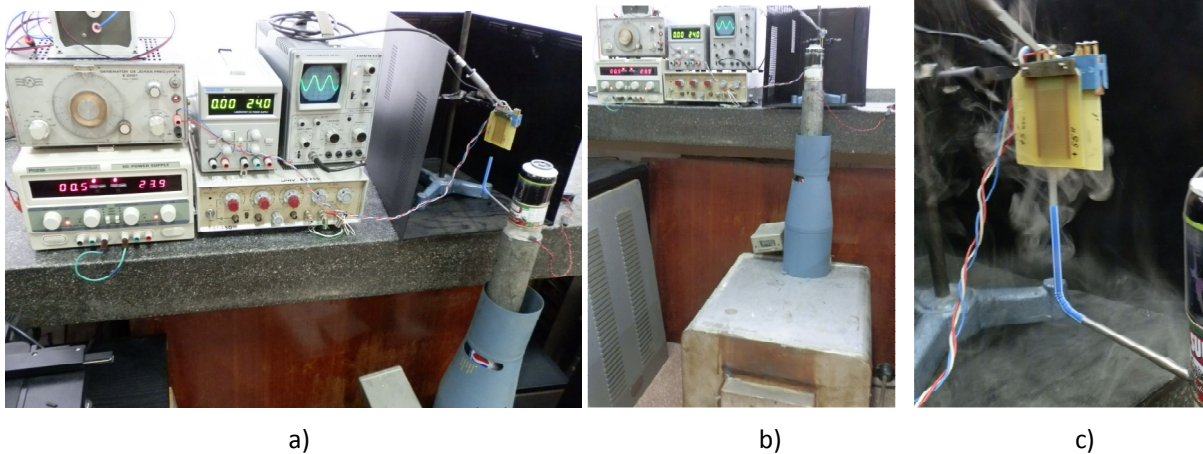


Figure 3: Experimental installation, a), combustion pilot plant, b), experimental device at work, c).

Figure 4a) shows the installation designed for the image analyses of the deposition plates, consisting in a metallographic microscope with CCD camera, and Figure 4b) the magnified image at 100x of a snapshot representing a clean deposition plate (in the absence of deposited nanoparticles due to fumigation). The vertical bright stripes are the electrodes and the dark stripes are areas between electrodes.

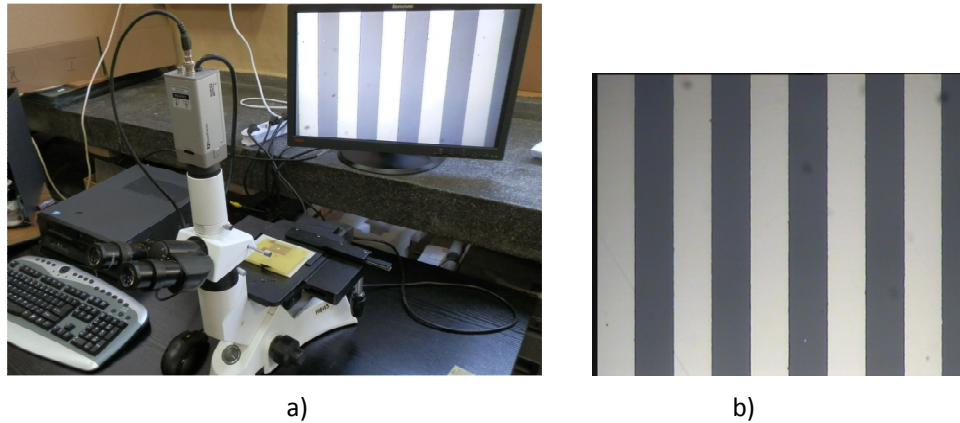


Figure 4: the installation for analysis of the deposition plates, a), magnified image at 100x of a snapshot representing a clean deposition plate, in the absence of the nanoparticle deposition b).

Tests have shown that, in the absence of applied voltage on the electrodes, the nanoparticles that exist in the flue gases are not attracted to them and, therefore, will not be deposited on the plates. By applying an AC voltage the deposition phenomenon occurs due to positive dielectrophoresis.

Figure 5 shows successive video frames (snapshots) representing the deposition of nanoparticles on the collection plates by pDEP of the smoke resulted from the incineration of 3 types of wastes in the pilot plant (samples A, B, C).

On the electrodes was applied an AC signal, with $U=24V$, $f=50Hz$, and fumigation time $t=30s$. Snapshots were performed at different distances from the top of the plate, where obtained a minimum density of the collected material versus the bottom, where the density of deposited nanoparticles is the greatest. It shows a decreasing in the concentration of nanoparticles captured, vertically from the entrance toward the exit area. As the smoke "climb" the device are lost particles in suspension by their accession to the collection plate, the result being in accordance with numerical simulations.

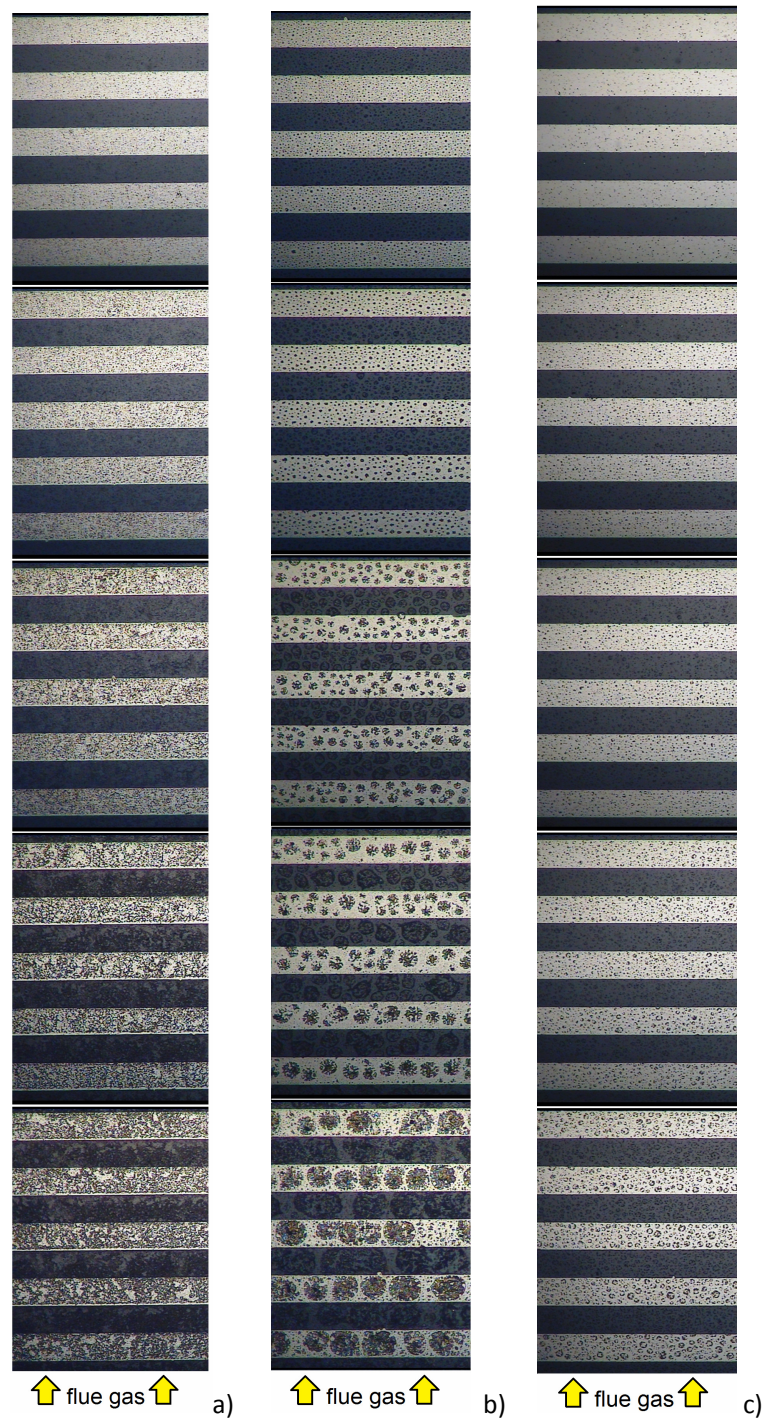


Figure 5: Comparative results for samples A, B, C, obtained by applying the results of activity 1.2 on the establishment of efficient regimes for the capture of nanoparticles, in order to minimize their emissions into the atmosphere. successive video frames (snapshots) representing the deposition of nanoparticles on the collection plates by pDEP of the smoke resulted from the incineration of 3 types of wastes in the pilot plant: probe A, a), probe B, b), probe C, c). On the electrodes was applied an AC signal, with $U=24V$, $f=50Hz$, and fumigation time $t=30s$. A decreasing in the concentration of captured nanoparticles, vertically from the entrance toward the exit area is observed.

a. Chemical analyses

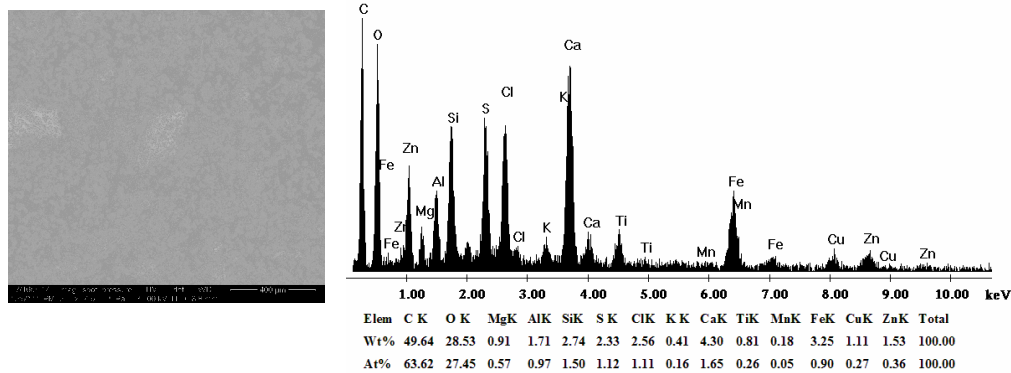
As the amount of particles deposited on the plates are very small, to determine the composition were analyzed ashes remaining after burning samples. Table 1 presents the AAS analyses performed with a KONTRAA 700 spectrophotometer, revealing the metallic and total organic carbon (TOC) contents of the samples.

Table 1: Metallic and total organic carbon (TOC) contents of the samples.

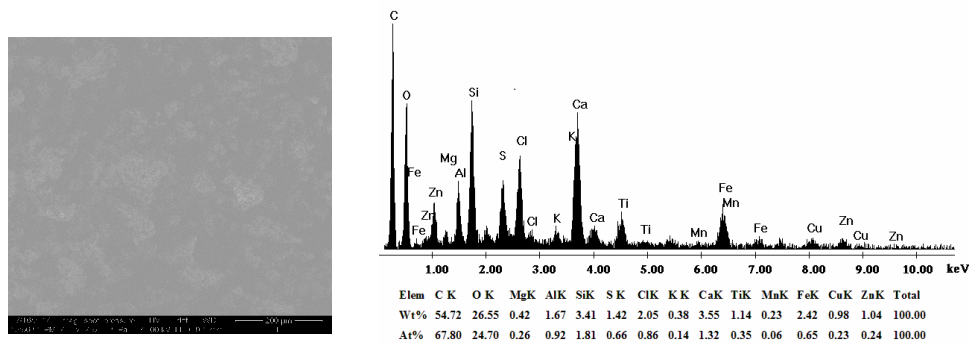
| Elements | Content | | | | | |
|----------|---------|-------|---------|-------|---------|-------|
| | Probe A | | Probe B | | Probe C | |
| | mg/kg | % | mg/kg | % | mg/kg | % |
| Al | 21980 | 2.2 | 17980 | 1.8 | 15980 | 1.6 |
| Cd | 3000 | 0.003 | 6000 | 0.006 | 5000 | 0.005 |
| Co | - | - | - | - | - | - |
| Cr | 758 | 0.076 | 198 | 0.02 | 178 | 0.18 |
| Cu | 790 | 0.8 | 590 | 0.6 | 790 | 0.8 |
| Fe | 24460 | 2.45 | 15980 | 1.6 | 14980 | 1.5 |
| Mn | 600 | 0.06 | 400 | 0.04 | 400 | 0.04 |
| Ni | 200 | 0.02 | 718 | 0.072 | 2890 | 0.29 |
| Pb | 3390 | 0.34 | 159 | 0.16 | 290 | 0.3 |
| Sb | - | - | - | - | - | - |
| Zn | 15980 | 1.6 | 7890 | 0.79 | 16460 | 1.65 |
| TOC | 32980 | 3.3 | 27980 | 2.8 | 25980 | 2.6 |

b. Morphological characterization of samples by scanning electron microscopy (SEM) and their elemental analysis by X-ray energy dispersive spectroscopy (EDAX)

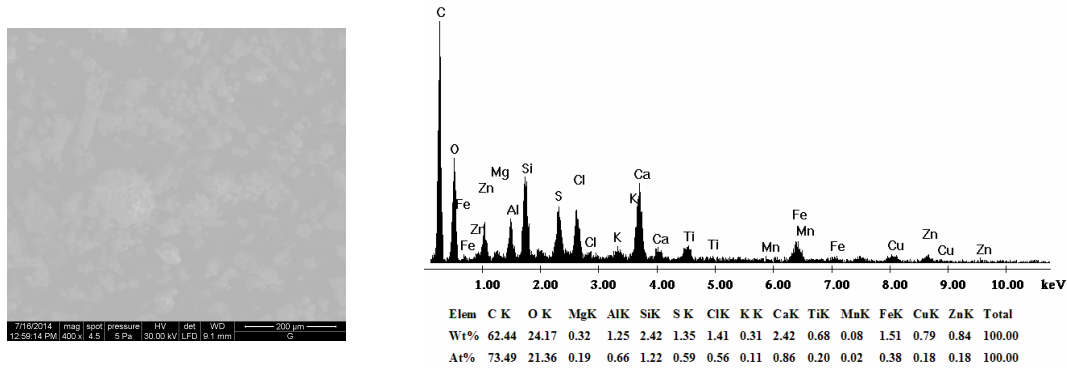
In the case of investigated samples, the results are presented in Figure 6:



Probe A



Probe B



Probe C

Figure 6: SEM micrograph of the samples and the results of elemental analysis by EDAX electron microscopy for evidence of ashes investigated.

c. Dimensional characterization using NanoSight LM 10 system

For dimensional characterization of the nanoparticles deposited on the plates after fumigation, they were collected by washing plates with distilled water for each of the three samples mentioned above. We performed several experiments of deposition/collection of suspensions of nanoparticles from flue gas resulting from the incineration of different wastes, but we present only the three considered to be representative.

We analyzed the particle size/concentration distribution using a Nano Sight LM 10 nanoparticle visualization system, based on nanoparticle-tracking analysis method.

- Probe A

Figure 7 illustrates the particle size/concentration distribution for the probe A. The distribution diagram indicates that it contains three significant groups of nanoparticles, having sizes of 27 nm, 105 nm and 240 nm.

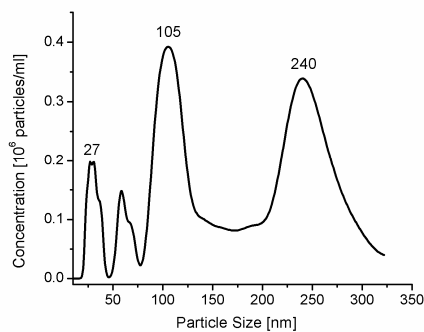


Figure 7: Particle size/concentration distribution diagram for probe A.

- Probe B

Figure 8 illustrates the particle size/concentration distribution for the probe B. The distribution diagram indicates three significant groups of nanoparticles, having sizes of 73 nm, 128 nm and 220 nm.

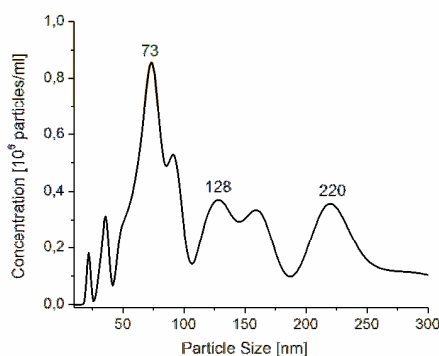


Figure 8: Particle size/concentration distribution diagram for probe B.

- Probe C

Figure 9 illustrates the particle size/concentration distribution for the probe A. The distribution diagram indicates three significant groups of nanoparticles, having sizes of 28 nm, 54 nm and 251 nm.

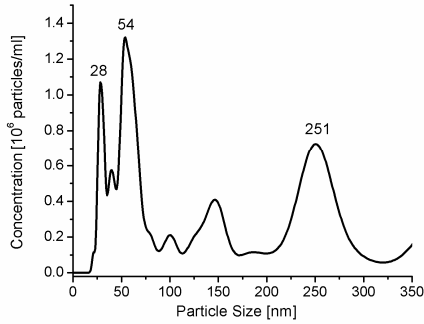


Figure 9: Particle size/concentration distribution diagram for probe C.

In summary, as can be seen from the analysis reports generated by the software LM 10, for each of the 3 samples were obtained significant size range of nanoparticles having values between 27 nm - 251 nm, which shows that all collected samples contain nanoparticles.

- Establishing of efficient regimes in nanoparticles manipulations to minimize their emission in the atmosphere.

- Feed-back on the improvement of the mathematical model and experimental for improving the used mathematical models, optimization of the experimental systems and the process parameters for the retention of the nanoparticles.

Based on the obtained results, was performed a numerical study in order to improve the filtering process of nanoparticles in suspension in flue gas inside a microfluidic separation device using positive dielectrophoresis. We have investigated the nanoparticles with sizes between 50-100 nm. The numerical simulations were performed with COMSOL Multiphysics software based on finite element method, acquired in the project. We considered the relative permittivity of flue gas $\epsilon_r \sim 1$. For the analysis of the filtration process we define the novel quantity named *Filtration rate (F)*, which describes the process in terms of nanoparticles entrapment at the electrodes, related to the concentration distribution:

$$F = \frac{C_{input} - C_{output}}{C_{input}} = 1 - C_{output} / C_{input} \quad [\%] \quad (1)$$

where C_{input} and C_{output} are the mean concentrations of suspended nanoparticles at the input and the output surfaces of the device, respectively, as schematically sketched in Figure 10.

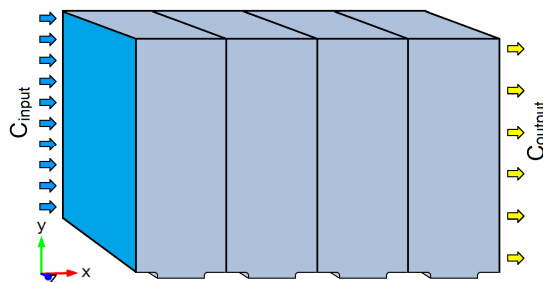


Figure 10: Schematic representation of the separation device revealing the parameters used for defining the *Filtration rate*.

For the computation of the pDEP force, we first solved the Laplace equation for the real and imaginary components of the electric potential, together with the associated boundary conditions [3,7,13]. The computational domain consists of a unit cell described by the following set of geometric parameters: $d=l=100 \mu\text{m}$ and $h=2 \text{mm}$. The simulations were performed for a suspension of particles with characteristic sizes $a=50\text{nm}$, $a=100\text{nm}$ and $a=200\text{nm}$ respectively, in air. The dielectric response of the particles is characterized by the real part of the CM factor $K_R = 1$ and we considered the amplitude of the electric potential applied on the electrodes in the range $U = 12 \div 24\text{V}$. The efficiency of the filtration

process can be evaluated by calculating the *Filtration rate* (4) for different values of problem's parameters. The computation is performed using an iterative procedure: the output concentration in one unit cell is considered the input concentration for the next unit cell, in order to describe the cumulative effect of the filtration inside the dielectrophoretic device. This type of analysis allows an estimation of the necessary number of cells (or electrodes) in order to obtain a certain desired filtration rate, when the other parameters of the problem are fixed.

The results presented in Figure 11 a) show that in the case of particle having size of 100nm, a desired filtration rate of 90% can be obtain by using about 30 electrodes when applying a voltage of 24 V, about 60 electrodes for 18 V, and nearly 200 electrodes for an applied voltage of 12 V. Figure 11 b) shows variation of filtration rate depending on the radius particles to an applied voltage $U = 24V$. As expected, is observed that the retaining of the particles on electrodes increases with their radius the number of cells.

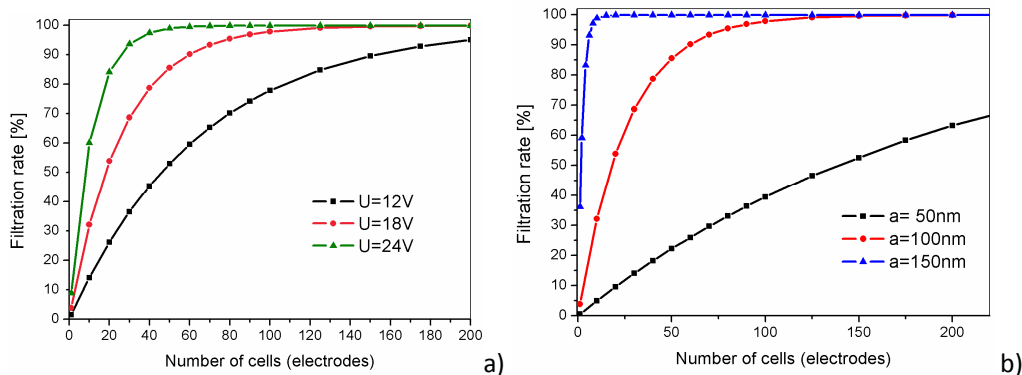


Figure 11: Calculated filtration rate versus number of cells for a) particles with $a=100nm$ at three different applied voltages and b) particles with three different radii at a fixed applied voltage of $U = 24V$ ($d = l = 100 \mu m$, $h = 2 mm$).

In summary, such simulations allow estimation of filtration efficiency depending on physical and geometrical parameters of the problem being very useful for the optimizing of the system by establishing effective arrangements for the capture of nanoparticles, in order to minimize their emissions into the atmosphere.

Conclusions

Based on the results obtained from mathematical modeling and numerical simulations from previous stages, was designed, developed and tested a laboratory microfluidic device for retaining in nonuniform electric field by positive dielectrophoresis of nanometric particles from the emissions of a pilot plant incinerator by burning specific categories of waste incinerator Pro Air Clean Timisoara.

Experiments showed deposition of nanoparticles on the electrode, the concentration of captured particles decreasing as we move away from the entrance area of the smoke resulted from the combustion of different wastes, the practical results being in good agreement with simulations.

Was performed a numerical study on the effectiveness of filtering nanoparticles from combustion gases in a microfluidic device designed to improve the filtering process of nanoparticles in suspension in flue gas using positive dielectrophoresis. This type of analysis allowed an estimation of the number of cells (or electrodes) required to achieve a given filtration rate when other parameters of the problem are established. Thus, if the particle size is 100 nm, a desired filtering rate of 90% can be obtained by using 30 electrodes when applying a voltage of 24 V, and about 200 electrodes when applied voltage is 12 V

9. Dissemination of the obtained results.

The obtained results were disseminated in the frame of three international conference, three papers published and two submitted for publication in ISI journals and three chapters in a book published by Springer Publishing House, whose book publishers are the project manager and two of the team members as listed below. All publications contain acknowledgment of the project. During the stage the project website was constantly updated, at the address: www.nanodep.com.

Conference participations:

- [1] A. Neculae, M. Bunoiu, A. Lungu and M. Lungu: *Flue gas filtration prediction in microfluidic devices using dielectrophoresis*, The 14-th International Balkan Workshop on Applied Physics, Constanta, July 2-4-, 2014.
- [2] A. Neculae, M. Bunoiu, A. Lungu and M. Lungu: *Electrohydrodynamic filtration of flue gas by nanoparticle trapping in microfluidic devices*, ICPAM-10, 10th International Conference on Physics of Advanced Materials, Iasi, Romania, 21-26 September 2014, Iasi, Romania.
- [3] A. Neculae, A. Lungu, M. Bunoiu and M. Lungu: *Nanoparticles trapping from flue gas using dielectrophoresis*, TIM-14 Physics Conference – Physics without frontiers, Timisoara, Romania, November 20-22, 2014.
- [4] J.M. Patrascu, M. Bunoiu and M. Lungu: *The nanoparticle effect hypothesis in femoral head aseptic necrosis*, TIM-14 Physics Conference – Physics without frontiers, Timisoara, Romania, November 20-22, 2014.

ISI Publications:

- [5] A. Neculae, R. Giugiulan, M. Bunoiu and M. Lungu: Effects of flow velocity upon nanoparticle distribution in microfluidic devices under dielectrophoresis, *Romanian Reports in Physics*, Vol. 66, No. 3, P. 754–764, 2014.
- [6] I. Malaescu, M. Lungu, R. Giugiulan and N. Strambeanu: The Clausius-Mossotti factor in low frequency field of the powders resulted from waste combustion, *Rom. Jour. Phys.*, Vol. 59, Nos. 7–8, P. 862–872, 2014.
- [7] M. Lungu, S. Balasoiu, M. O. Bunoiu and A. Neculae: Study of a 3D DEP-based microfluidic system for selective nanoparticle manipulation, *AIP Conference Proceedings 1634*, Melville, New York, p. 89-94, 2014.
- [8] A. Neculae, M. Bunoiu, A. Lungu and M. Lungu: Filtration of flue gas in microfluidic devices using dielectrophoresis, *Romanian Reports in Physics (accepted)*.
- [9] M. Lungu, I. Malaescu, N. Strambeanu and A. Neculae: Assessment on separation of nanoparticles from flue gas using dielectrophoresis, *J. Nano. Res.* (under review).

Books:

- [10] M. Lungu, A. Neculae, M. Bunoiu and C.G. Biris (editors): ***Nanoparticles' Promises and Risks; Characterization, Manipulation, and Potential Hazards to Humanity and Environment***, Springer Science+Business Media, ISBN: 978-3-319-11727-0 (Print) 978-3-319-11728-7 (Online), 355 pagini, 2014.

Book Chapters:

- [11] N. Strambeanu, L. Demetrovici, D. Dragos and M. Lungu, Chapter I: *Nanoparticles: Definition, Classification and General Physical Properties*, Part I: Nano-particle Classification and Sources in Human Society, Book: **Nanoparticles' Promises and Risks; Characterization, Manipulation, and Potential Hazards to Humanity and the Environment**, Springer Science+Business Media, ISBN: 978-3-319-11727-0 (Print) 978-3-319-11728-7 (Online), p. 3-9, 2014.
- [12] A. Lungu, M. Lungu, A. Neculae, R. Giugiulan, Chapter 13: *Nanoparticle Characterization Using Nanoparticle Tracking Analysis*, Part III: Characterization and Detection Methods for Nanoparticles, Book: **Nanoparticles' Promises and Risks; Characterization, Manipulation, and Potential Hazards to Humanity and the Environment**, Springer Science+Business Media, ISBN: 978-3-319-11727-0 (Print) 978-3-319-11728-7 (Online), p. 245-271, 2014.
- [13] M. Lungu, M. Bunoiu and A. Neculae, Chapter 14: *Dielectrophoresis Used for Nanoparticle Manipulation in Microfluidic Devices*, Part IV: Methods for Sorting, Separating and Manipulating Nanoparticles, Book: **Nanoparticles' Promises and Risks; Characterization, Manipulation, and Potential Hazards to Humanity and the Environment**, Springer Science+Business Media, ISBN: 978-3-319-11727-0 (Print) 978-3-319-11728-7 (Online), p. 271-303, 2014.

Project manager,
Dr. Mihai LUNGU
Associate Professor,
Physics Faculty,
West University of Timisoara